To the Graduate Council:

I am submitting herewith a thesis written by Sumeet Kaul entitled "Insight into the Gating Mechanism of Mechanosensitive Ion Channels using a simple structure: A step in the analysis of c*ommotio cordis*" I have examined the final electronic copy of this thesis for form and content and recommend that it be accepted in partial fulfillment of the requirements for the degree of Master of Science, with a major in Biomedical Engineering.

Xiaopeng Zhao, Major Professor

We have read this thesis
and recommend its acceptance:

J.A.M Boulet

Allen J. Baker

Accepted for the Council:

Carolyn R. Hodges, Vice Provost and
Dean of the Graduate School

(Original signatures are on file with official student records.)

Insight into the Gating Mechanism of Mechanosensitive Ion Channels using a simple structure: A step in the analysis of *commotio cordis*

A Thesis Presented for
the Master of Science
Degree
The University of Tennessee, Knoxville

Sumeet Kaul
August 2009

Copyright © 2009 by Sumeet Kaul
All rights reserved.

Acknowledgements

I would first like to thank my parents, Satish and Kavitha Kaul and my sister Moneca Kaul, who have always encouraged, supported and believed in me throughout my academic life. I would like to thank Marissa Rodrigues without whom this work would have been impossible. I also would like to thank Dr. Zhao for his steady support and unbiased opinion during the tenure of my research. Lastly, I want to thank Dr. Baker and Dr. Boulet for helping me generously in the last leg of my graduate studies.

Abstract

Mechanosensation in cells is a well known phenomenon that is associated with cellular responses to force. Our knowledge of the trigger mechanism of this phenomenon is, however, limited. Earlier studies in this field have used atomic simulations, which although being accurate, are limited in their feasibility in multi-length scenarios like a mechanosensitive channel that undergoes micro-level changes in the composition of the protein to cause a macro-level change in the state of a biological structure such as the muscle. Finite Element Analysis has been used in various engineering fields to study the mechanical response of complex structures. The current study is a step in utilizing the phenomenal capabilities of Finite Element Analysis in developing and studying a 3D model (Membrane-Channel) of a mechanosensitive channel of large conductance (MscL). A simplified CAD structure of *Mycobacterium tuberculosis* (*TbMscL*) was developed in the first stage of this study. The authenticity of this model was tested by applying two types of loading conditions, namely (i) In-plane stretch and (ii) Out-of-plane bending. The results obtained from the first step of analysis are in accordance with previous experimental data, which elucidates the fact that tension within the membrane guides the gating mechanism of the channel and not the curvature of the membrane. The second stage of the analysis involved the use of the same model to study the disease c*ommotio cordis*. This was achieved by calculating the loading conditions during the onset of the condition in the human heart and then transferring those conditions to the Membrane-Channel model developed in the first stage. The result showed that although the channel did not fully open but there was a significant change in the channel's radius that might cause the flow of ions, thereby changing the state of the channel. It is anticipated that this model will help future research in areas that conventionally have been difficult to model.

Table of Contents

Acknowledgements iii

Abstract iv

List of Tables vii

Table of Figures viii

CHAPTER I Introduction 1

Problem statement 5

CHAPTER II The Effect of Mechanosensitive Channels on Ventricular Pathophysiology:

commotio cordis 6

2.1 Experimental Models of Cardiac Mechanosensitivity 7
2.2 Theoretical Cardiac Modeling of commotio cordis 8
The earliest three-dimensional cardiac model used to study arrhythmias was developed by 8

CHAPTER III Finite Element Modelling of Gated Mechanosensitive Channels 17

3.1 Continuum-based Simulations and Mechanobiology 17
3.2 Gating Mechanism of the Mechanosensitive Channel of Large Conductance (MscL): Insights from Continuum-based FEM Simulations Developed by Tang and coworkers 18
3.2.1 The FEM Model 18
3.2.2 Gating Mechanism of MscL 20
3.2.2.1 MscL Gating upon Equi-biaxial Tension 20
3.2.2.2 MscL Gating upon Bending 22
3.2.2.3 Contribution of the Structural Motifs to MscL Gating 22

CHAPTER IV FEM Modeling of TbMscL using Autodesk® AutoCAD 2007 & ABAQUS® .. 25

4.1 The Geometry 25
4.2 The Helices 27
4.2.1 TM1 & TM2 Helices 27
4.2.2 Radius of the Channel 30
4.3 The Membrane 30
4.4 The Membrane-channel Combine 31
4.5 The Two-channel Membrane-channel Model 34
4.6 The Heart 35
4.7 Meshing 35

4.7.1 Membrane-Channel Model 36
4.7.2 Two-channel Membrane Model 37
4.7.3 The Heart 37

CHAPTER V Results 43

5.1 Membrane-channel Model 43
5.1.1 Boundary Condition 43
5.1.1.1 In-plane Stretching 43
5.1.1.2 In-plane stretching - Two-channel Model 44
5.1.1.3 Out-of-plane Bending 44
5.1.1.4 Out-of-plane Bending - Two-channel Model 44
5.1.2 The Loads 44
5.1.2.1 In-plane Stretch 44
5.1.2.2 In-e stretch- two channel Model 49
5.1.2.4 Out-of-plane Bending - Two-channel Model 50
5.1.2.3 Out-of-plane Bending 51
5.1.3 Results of the Analysis 54
5.1.3.1 In-plane Stretch 54
5.1.3.2 In-plane Stretch - Two-channel Model 58
5.1.3.3 Out-of-plane Bending - +ve Z-direction 58
5.1.3.4 Out-of-plane Bending - -ve Z-direction 65
5.1.3.5 Out-of-plane Bending - +ve Z-direction - Two-channel Model 65
5.1.3.6 Out-of-plane Bending - -ve Z-direction - Two-channel Model 71
5.2 The Heart Model 71
5.2.1 Boundary Conditions 71
5.2.2 Applied Loads and Results 76
5.3 Discussion of Results 78

CHAPTER VI Future Directions 82

List of References 83

Vita 90

List of Tables

Table 1: Summary of Geometric Properties of the Helices 30
Table 2: Geometric Properties of the Membrane Model 33
Table 3: Geometric Properties of the Two-channel Membrane Model 36
Table 4: Material Properties of the Features of the Membrane–channel Model. 38
Table 5: Differences in the Properties of the Actual and the Modified Heart Model. 42
Table 6: Results of In-plane Stress Analysis 57
Table 7: Results of the Analysis 62
Table 8: Results of the Analysis 64
Table 9: Results of the Analysis 67
Table 10: Results of the Analysis 70
Table 11: Results of the Analysis 74
Table 12: Results of the Analysis 80

Table of Figures

Figure 1: (a) Top view of the open state structure of the mechanosensitive channel MscL. (b) Side views of the MscL channel depicting the TM domains and the inset shows the monomeric structure of the channel together with the interconnecting loop. (Boris Martinac, (2004)). 3

Figure 2: ECG from an anaesthetized pig subjected to precordial baseball impacts (commotio cordis) demonstrating that arrhythmia is affected by impact timing relative to the cardiac cycle. Adopted from Link et al. (1998). 7

Figure 3: A significant increase in whole cell current due to activation of K^+ ATP in guinea pig ventricular myocytes. Figure adopted from Kohl et al. (2006)..... 9

Figure 4: The 2D ventricular tissue slice model developed by Kohl et al (2004) in a 2.5 cm X 2.5 cm mesh. Figure adopted from Kohl & Garny, (2004)..... 12

Figure 5: 3D Rabbit ventricular model developed by Li et al. (2004). This figure illustrates the evolution of transmembrane potential after a 140ms impact. Figure adopted from Li et al. (2004). 13

Figure 6: 3D ventricular free wall model developed by Garny et al. This figure illustrates the sustained arrhythmia following a mechanically induced stimulation in the early T-wave window. Figure adopted from Garny et al. (2005). 15

Figure 7: Top and side view of the closed state of the *E.coli* MS channel FEM model. (Figure from: Tang et al. (2008))..... 19

Figure 8: (a) The finite element mesh for the lipid bilayer membrane embedded with *E.coli* MscL during equi-biaxial tension. (b) The assembled continuum structure of an *E.coli* MscL inside a lipid bilayer. The inset illustrates the cavity created to accommodate the MscL. Figure adopted from Tang et al. (2008). 21

Figure 9: Comparison of the gating transition pathway of MscL obtained by the structural model developed by Sukharev et al and the FEM model developed by Tang et al. Figure adopted from Tang et al. (2008). 23

Figure 10: Pure bending of the membrane does not increase the radius of the channel pore significantly. Figure adopted from Tang et al. (2008). 24

Figure 11: Effects of removing structural components of the MscL channel on gating behaviour. Panel 1 represents the full protein without any structural motifs cut. Figure adopted from Tang et al. (2008). 24

Figure 12: Structural and Finite Element model of the channel. (a, b) Top and side structural views of the channel (c, d) Top and side views of equivalent FEM model. Figures (a) and (b) have been adopted from Tang et al. (2006). 26

Figure 13: 3D CAD models of TM1 and TM2 helices with their dimensions. 28

Figure 14: 3D views of the TM1-TM2 helix combine. (a), (b) and (c) show the top view, side view and front view of the combine respectively. 29

Figure 15: The Radius of the Channel; the current figure depicts a hypothetical cylinder with radius ‘r’ that represents the radius of the channel. 31

Figure 16: (a) and (b) represent 2D views of the membrane with the dimensions. (c) represents the 3D view of the structure. 32

Figure 17: The Membrane-channel combine. (a), (b), (c) represent the different geometric views of the model. (d) gives a closer look at the TM2 helix-membrane integration. 34

Figure 18: (a), (b) represent the dimensions of the two-channel model in 2D. (c) represents a 3D view. 36

Figure 19: Different views of the heart model. (a) posterior view, (b) anterior view, (c) top view and (d) bottom view. 38

Figure 20: Membrane-channel model mesh. (a), (b) and (c) respectively, illustrate 2D front, side and 3D cross view of the meshed combine. (d) demonstrates the visual of the mesh profile around the channel. 39

Figure 21: Membrane - two-channel model mesh. (a), (b) and (c) respectively, illustrate 2D front, side and 3D cross view of the meshed combine. 40

Figure 22: Pre and Post mesh views of the heart model. (a) anterior view before the mesh, (b) anterior view after the mesh, (c) top view before the mesh and (d) top view after the mesh. 41

Figure 23: Boundary conditions applied for the in-plane stretch mode on the membrane-channel model 45

Figure 24: Boundary conditions for the in-plane stretch mode of the two-channel model. 46

Figure 25: Out-of-plane bending deformation applied on the membrane channel model 47

Figure 26: Out-of-plane bending deformation applied on the two-channel model. 48

Figure 27: Force applied to the outer edge of the membrane. The magnitude of the force is 35MPa. It increases exponentially from 0 to the maximum load over the time period of the simulation. 49

Figure 28: In-plane bending deformation of 35 MPa applied to the two-channel model. 51

Figure 29: Out-of-plane bending applied to the membrane channel model in the positive and negative Z-direction. 52

Figure 30: Out-of-plane bending deformation applied on the two-channel model. 53

Figure 31: Gating transition of the membrane channel at different time points (t=0 through t=1 s). 57

Figure 32: Gating transition of the two-channel model at different time points (t= 0 through 1 s). 61

Figure 33: Gating transition at different time points (in sec) after application of out of plane bending in the +Z direction to the membrane channel model. 63

Figure 34: Gating transition at different time points (in sec) after application of out of plane bending in the -Z direction to the membrane channel model. 67

Figure 35: Gating transition at different time points (in sec) after application of out-of-plane bending in the +Z direction to the two channel model. 70

Figure 36: Gating transition at different time points (in sec) after application of out-of-plane bending in the -Z-direction to the two-channel model. 74

Figure 37: (a), (b) and (c) represent different three-dimensional views of boundary conditions applied to the heart model. 75

Figure 38: Impact on the chest at various points. 77

Figure 39: Applying the results of the Heart analysis to the Membrane-Channel model. Figure presents frames at t= 0 through 1 s. 80

CHAPTER I Introduction

Mechanosensation represents a sensory transduction process evolved by cells to respond to a wide range of mechanical stimuli. Mechanosensation is attributed to the presence of cell membrane-localized gated mechanosensitive (MS) ion channels that convert external mechanical forces into electrical or biochemical signals. These signals can then transduce intracellularly to regulate physiological processes such as touch, hearing (Martinac, (2004)), cutaneous depression, muscle spindle elongation, aorta distension (Sukahrev, (2004)) and even prokaryotic processes such as adaptation to osmotic stress (Stokes, Murray & Subramaniam, (2003)) and cellular turgor control during cell division and growth (Levina et al. (1999)). Typically, when the cell membrane is perturbed by some form of mechanical distortion, MS channels undergo an alteration in conformation which triggers a change in the conductance of the channel thus leading to either depolarization or hyperpolarization of the cell membrane. This conformational change modulates the cation-transporting activity of the channel by opening or closing the channel through distortion of the associated lipid bilayer and in this manner a mechanical signal is converted to a biochemical cellular response (Ingber, (2006)).

MS channels are expressed in several cell types and tissues including the heart, brain, muscles, retina, neurons and they play an important role in modulating patho-physiological conditions such as muscular degeneration (Franco and Lansman, (1990); Teichmann, (2009)), Human Bartter syndrome IV (Rickheit et al., (2008)), hypertension (Kohler et al., (1999)), cardiac arrhythmias (Franz et al., (1992); Maroto et al., (2005); Ninio et al., (2008)) and polycystic kidney disease (Chen et al.,1999). For example, stretch activated cation channels (SA-CAT channels) found in cardiac tissue have been shown to produce arrhythmogenic electrophysiological changes during stretch and mechanical dysfunction of the heart (Franz et al., (2003); Sachs, (2004)). The inward passage of Ca^{2+}, K^{+} and Na^{+} ions through the SA-CAT channels during stretch induces the maintenance of atrial fibrillation (Franz et al., (2003)).

Despite the identification of several MS ion channels in prokaryotic and eukaryotic cells, the detailed mechanism by which MS channels sense mechanical stress and convert them to biological signals remains to be elucidated. Much of the information into how MS channels function has come from computer simulation studies that allow for exploring these systems on multiple lengthscales and timescales. Advances in biological imaging and micromanipulation have enabled the identification of critical mechanosensitive molecules and cellular components, but these techniques are limited by the fact that different modes of membrane deformation exist and trying to characterize these conformational changes experimentally at the quantitative level can be difficult. For this reason computer modeling provides an invaluable tool in analyzing the multi-scale nature of biomechanical problems (Tang et al., (2006)).

Amongst the several putative MS channels that have been identified, the most well characterized ones are the large conductance mechanosensitive channels (MscL) of prokaryotes. MscL was first isolated from the intestinal bacterium *Escherichia coli* where it functions as an inner membrane stretch-activated osmotic release valve (Sukharev et al., (2004)). MscL exists in a pentameric form and spans the membrane twice through its transmembrane helices- TM1 and TM2 (Figure: 1a). TM1 and TM2 are interconnected by an extracellular periplasmic loop (Figure: 1b). In 1998, Rees and coworkers (Chang et al) resolved the three-dimensional crystal structure of the MscL protein channel in the pathogenic bacterium *Mycobacterium tuberculosis (Tb).* Sukharev and others built a model of the *E.coli* MscL by homology to the structure of *Tb*MscL (Sukharev et al., (2004)). In their model, the TM1 helices form the core of the transmembrane bundle and they make up the hydrophobic gate of the MS channel (Figure: 1a). The TM2 helices are aligned along the periphery of the channel and they face the lipid environment. According to this model, in response to membrane tension, the MscL opens a water-filled pore of about 3nm in diameter that is lined by TM1 helices (Perozo et al., (2002)). This gating transition is predicted to be mediated by a tilting of the transmembrane helices thus causing the expansion and flattening of the channel. A series of 13 conformational states was constructed for the gating transition of both *E.coli* and *Tb* MscL (Sukharev et al). A few studies have been published using targeted molecular dynamics and equilibrium molecular dynamic

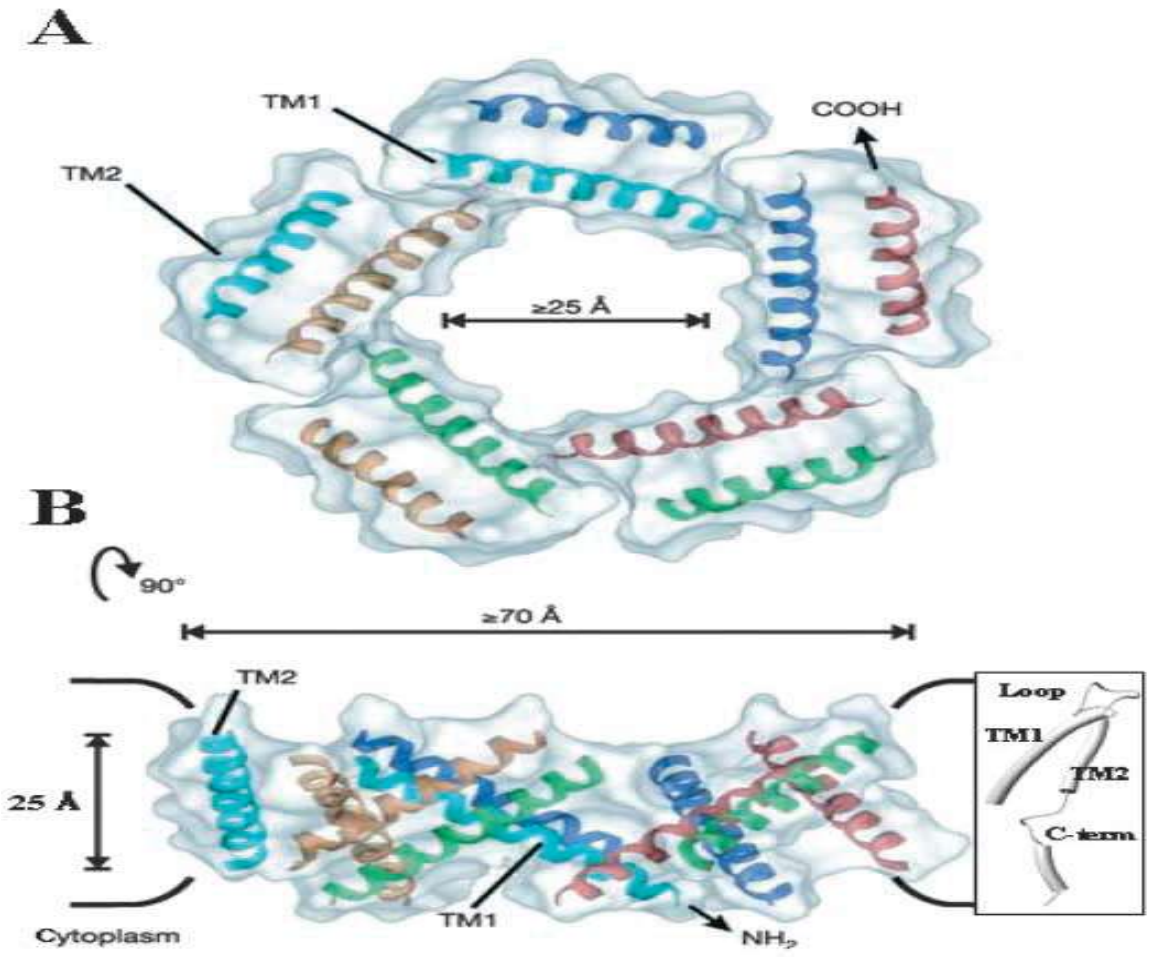


Figure 1: (a) Top view of the open state structure of the mechanosensitive channel MscL. When a membrane tension acts at the ends of the TM helices, the hydrophobic gate formed by the TM1 helices expands in an iris-like manner resulting in hydration of the central pore and opening of the channel to a low-conducting conformation.

(b) Side views of the MscL channel depicting the TM domains and the inset shows the monomeric structure of the channel together with the interconnecting loop. (Boris Martinac, (2004)).

simulations to yield helpful insights into the mechanisms of mechanotransduction, more specifically to analyze the gating mechanism. Although these atomistic simulations can be manipulated in a well defined way to simulate and design new experiments, they have certain limitations. For example, in one study by Gullingsrud et al. (2001), molecular dynamics (MD) simulation was applied to study the gating of *Tb*MscL. In addition to being limited by the time-scale for the simulation (occurring at nanometer scales and nanosecond events), the channel did not open to the pore radius proposed by other models (Sukharev, (2004)). Moreover, the targeted MD approach used by Kong et al. (2002) and Bilston et al. (2002) uses unrealistic constraining forces that leads to unrealistic structural transitions and protein-lipid interactions (Tang, (2008)). Meyer et al. (2006) used a pre-curved lipid membrane to eliminate this problem, however with this approach too, the pore size is significantly smaller and gating transition was observed even in the absence of external forces. Some investigators have even used different combinations of lipid headgroups and tails (Elmore et al., (2003); Debret et al., (2008)) to study the conformational changes in MscL and these studies helped confirm the importance of hydrophobic mismatching in the gating process. Despite advances in the all-atom simulations, this approach cannot be applied to realistic conditions since complex membrane deformations can only be introduced in nanometer scales and these approaches tend to be computationally intensive (Tang et al., (2008)).

Recently Tang et al. developed a continuum-mechanics model based on finite element mechanics that has proved to be the most effective in studying membrane deformations at multiple length scales and different deformation modes. This method can also be adapted to complex loadings and can include sufficient molecular details while maintaining some of the most important structural details and excluding redundant atomic details (Tang et al, (2008)). Tang and coworkers have used this approach to study mechanotransduction of both *E.coli* and *Tb* MscL. Simulations using their model can generate gating transitions that are in conformation with the current experimental data and all-atom simulations (Tang et al., (2006)).

For this thesis the model developed by Tang et al. was recreated and authenticated by comparing it with previous experimental results based on gating of *Tb*MscL obtained by Sukharev et al.

Furthermore, in order to display the effectiveness of finite element simulations in studying complex biological systems, this model was used in creating a mechanical impact profile associated with *commotio cordis* – a condition which results in sudden cardiac arrest following a blunt, low-impact chest wall trauma.

Problem statement

The aims of this thesis are:

1. Develop a finite element model of *TbMscl* based on previous experimental data.

2. Authenticate this model by comparing the results obtained in the simulation with existing data.

3. Perform a parameter study in the model under two conditions, namely, (i) in-plane stretch and (ii) out-of-plane bending.

4. Develop a two-channel membrane model and perform parameter study under two conditions, namely, (i) in-plane stretch and (ii) out-of-plane bending.

5. Perform stress analysis on a real 3D heart model, and apply the resultant stresses to the channel model developed in the earlier steps. This will help understand the mechanism of *commotio cordis*.

6. Provide future improvements/directions to the current area of research.

CHAPTER II The Effect of Mechanosensitive Channels on Ventricular Pathophysiology: *commotio cordis*

Commotio cordis is a condition that results in sudden arrhythmic death as a result of mechanical induction of heart rhythm disturbances that occur in the absence of structural damage to the chest and its organs during low-energy chest wall impacts such as those experienced by sportsmen. The idea that mechanical stimuli can affect the origin and the spread of cardiac electrical excitation arose in the late 1960's and more specifically Kohl et al. (1999) suggested that mechano-electric feedback can influence the induction of heart rhythm disturbances or their mechanical termination. The heart is a strong candidate for influence by mechanosensitive channels due to its continual and repetitive rhythmic contraction (Sachs and Bett, 2000). MS channels can influence many patho-physiological conditions of the cardiac tissue in addition to *Commotio cordis* such as arrhythmias (Craig & Hondeghem, (1990); Franz, (1995)), fibrillation, stretching of the cardiac membrane associated with myocardial infarction and changes in heart beat rate as a result of filling (Bainbridge, (1915)). Most of the evidence linking MS channels to cardiac arrhythmias has been derived from experiments that have utilized non-specific MS channel blockers such as gadolinium (Pascarel et al. (1998), Hansen et al. (1991)) to block stretch induced arrhythmias. Bode et al. (2001) used GsMTx-4, a small peptide found in venom of tarantulas to block stretch-activated MS channels and hence atrial fibrillation in perfused rabbit hearts.

In the case of c*ommotio cordis* (CC), the selective activation of a K^+ (ATP) channel has been implicated in the pathogenesis of ventricular fibrillation and is believed to be responsible for the sudden death associated with CC victims (Link et al. (1999)). In fact, Link et al showed that blocking of the mechanosensitive K^+ (ATP) channel by the pharmacological inhibitor glibenclamide reduced the incidence of ventricular fibrillation and the magnitude of ST-segment elevation using animal models of experimental CC (Link et al. (1999)). More recently the same investigators demonstrated that mechanical deformation of the cell membrane was pivotal to the activation of stretch-activated MS channels in CC (Link et al. (2008)). Thus literature linking mechano-electrical feedback and stretch activated channels to the sustenance of arrhythmias is

not scarce and is a topic of active research which warrants a more detailed understanding of the behavior of cardiac MS channels and their contribution to heart disease.

2.1 Experimental Models of Cardiac Mechanosensitivity

Whole-animal experiments became popular in the late 20th century and these studies challenged then-prevailing concepts of the mechanism of c*ommotio cordis.* Swine models of CC were used and ventricular fibrillation and ST-segment elevation were induced in the animals by 30-mph baseball impacts to the precordium (Link et al. (1999)). These studies revealed that arrhythmia associated with CC leads to ventricular fibrillation only when impacts are delivered 15ms prior to the peak of the ECG T wave (Figure 2, Link et al. (1998)).

As mentioned above, Link and coworkers also identified that activation of stretch-activated K^+ ion MS channels led to arrhythmias in the context of CC. Over the years precordial thumps

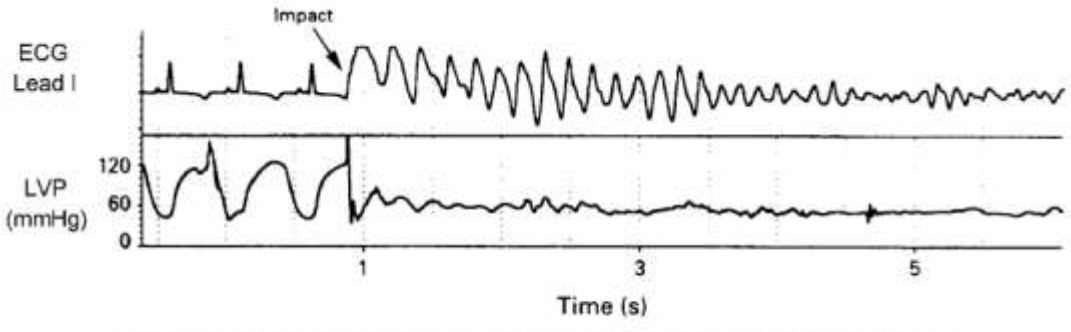


Figure 2: ECG from an anaesthetized pig subjected to precordial baseball impacts (commotio cordis) demonstrating that arrhythmia is affected by impact timing relative to the cardiac cycle. In this figure, the upper panel shows that the impact coincided with the first half of the T wave. In the lower panel, loss of left-ventricular pressure is associated with the swiftness of mechanical induction of ventricular fibrillation. Adopted from Link et al. (1998).

(Befeler, (1978); Kohl, et al. (2005)) and isolated hearts (Franz et al. (1992); Bode et al. (2001)) were used to study ventricular fibrillation in the context of CC. Recently, a soft tissue impact characterization kit has been developed to simulate isolated hearts in a controlled manner (Cooper et al. (2006)). This model system has proved to be effective in quantitatively characterizing probe-tissue interactions and is also well adapted to pharmacological interventions (Kohl et al. (2006)). Patch clamp techniques were also developed which involve applying mechanical simulation to a cardiomyocyte while simultaneously holding the cell under a voltage clamp. While this technique helped yield useful insights about the role of mechanosensitive channels in the myocardium (Wagoner, (1994)), as one can envisage, this method is associated with a lot of technical difficulties, especially with regards to maintaining cells in a physiologically active state throughout the simulation. Nonetheless coupling this method with other experimental techniques such as the carbon fiber method described by Le Guennec et al. (1990) has helped provide the link between cardiac membrane deformation and activation of K^+ ion channels. In one study, combining the carbon fiber method with simulated ischaemia confirmed that axial stretching of guinea-pig ventricular cardiomyocytes amplified the activation of the K^+ ATP channel (Figure: 3 Kohl et al. (2006)).

Experimental systems using simulated whole cells are not complex enough to represent all the features of the mechanotransduction pathway. Modifying the above mentioned model systems to mimic the complexity of biological systems would not be of any physiological value. Thus making any quantitative measurements on the cell poses a great limitation. This is where computer modeling has opened new ways to study membrane dynamics in atomic detail. The next section reviews some of the important contributions made using computer simulations to investigate mechanosensitive channels in the cardiac tissue.

2.2 Theoretical Cardiac Modeling of *commotio cordis*

The earliest three-dimensional cardiac model used to study arrhythmias was developed by

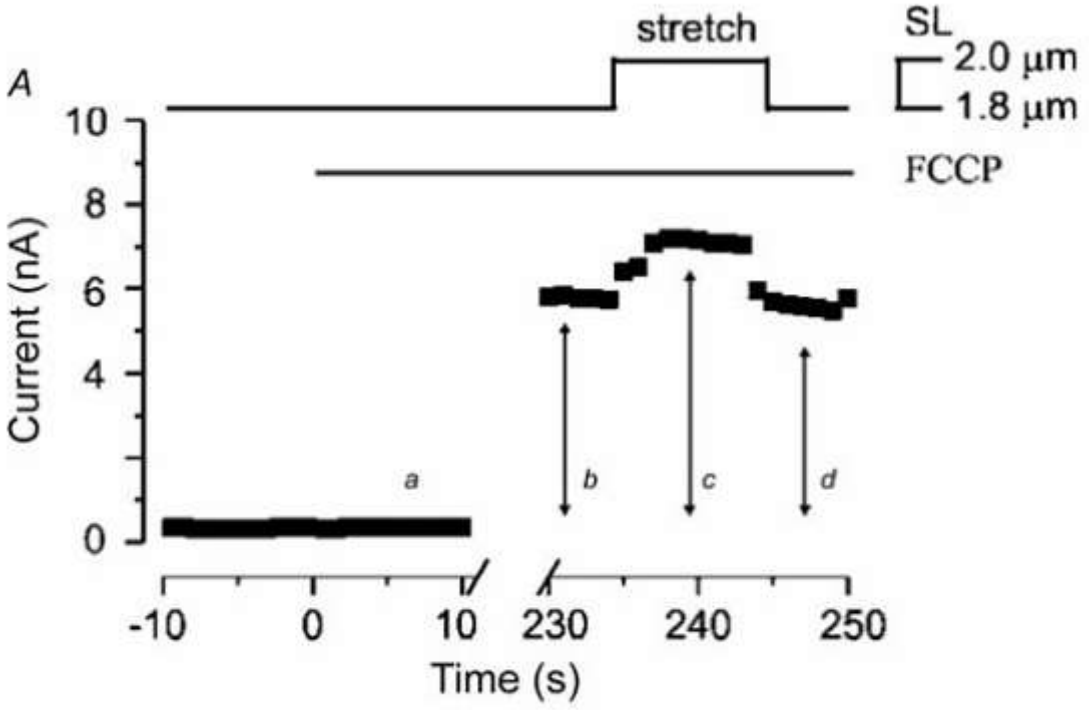


Figure 3: A significant increase in whole cell current due to activation of K^+ ATP in guinea pig ventricular myocytes. Figure adopted from Kohl et al. (2006).

Winslow et al. (1993) and since then computational modeling has come a long way. Advances in computer simulations have led to the development of the most anatomically detailed models of cardiac tissue architecture, representing almost every aspect of cardiac electrophysiology and mechanics (Garny & Kohl, (2005)). Several investigators have applied single-cell theoretical models to reproduce experimentally observed cardiac mechano-electrical interactions and to modulate mechanosensitive channels (Kohl et al. (1998); Kohl& Sachs, (2001); Markhasin et al. (2003); Healy & McCulloch, (2005). For example, Kohl et al. used the single-cell model approach to simulate sustained and transient diastolic/systolic stretch via mechano-electric feedback (MEF) in a Guinea pig ventricular cell model (1998). With this model they observed that activation of cation-non-selective stretch activated channels can trigger an action potential in resting cells and alter its duration. This result was then extrapolated to study the mechanism of *Commotio cordis* following mechanically-induced dysrhythmias and their work led to the identification of the role of stretch activated channels (SACs) in sustaining arrhythmias (Kohl et al., (2001)).

Simulation of CC in a 1 dimensional model is impractical since it is difficult to accommodate ventricular fibrillation in a 1D medium; hence most of the simulation studies have been conducted in 2D or 3D theoretical models (Garny & Kohl, (2005)).

Garny and Kohl (2004) developed a 2D mathematical model of the ventricular tissue to study the dynamic interactions of single cardiomyocytes subjected to mechanical simulation at different stages of repolarization. This model was supposed to mimic the *in vivo* tissue characteristics encountered upon precordial impact during the ECG T-wave (Garny & Kohl, (2004)). There were a lot of valuable insights provided by this model. Firstly, this model was the first to suggest that mechano-electric feedback could provide both the trigger and the sustenance mechanisms for arrhythmias via cation non-selective SAC activation which in turn led to the development of a region of functional block of conduction that was critical for the development of sustained reentry. Using this model it was also possible to model varying properties of mechanical stimuli on tissue repolarization by modifying the base and height of the tissue slice and also vary the timing of the impacts at different stages of tissue repolarization. Figure 4 illustrates how mechanical stimuli are effective in causing sustained arrhythmias if applied between 10% and

50% repolarization using the tissue slice 2D model developed by Kohl & Garny (2004). By modifying different parameters applied to this model, the same authors were able to identify that in order to sustain arrhythmogeneity, the timing of the impact has to coincide with the peak of the T wave, since impacts that coincide with early or late repolarization time-points (outside of the T wave peak) fail to induce sustained rhythmic disturbances. The explanation for this critical timing of impacts suggested by the model is that at early time-points (Figure: 4B), the mechanical stimulus cannot encounter sufficient tissue to form a focus of excitation and at later time-points (Figure: 4C) a large fraction of the tissue regains excitability and hence cannot support reentry of conduction (Garny & Kohl, (2004)).

While the 2D model study by Garny & Kohl suggested that recruitment of cation non-selective SACs triggered sustained arrhythmias and the K^+ selective SAC contributed to the development and sustenance of arrhythmias, the 3D model developed by Li et al (2004) sought to examine the induction of arrhythmia by the simultaneous recruitment of both types of SACs. This 3D model was built upon the rabbit ventricular model developed by Trayanova et al. (2003).

The rabbit ventricular model employed by Li et al. represented the heart architecture in a more realistic manner with respect to the geometry and fiber architecture. Moreover, the volume conductor modeled to fill the ventricular cavities had conductivity equal to that of blood. This model was ideal for the examination of cardiac defibrillation and membrane kinetics thus enabling modeling of SACs in a much more realistic manner. Simulations with this model reassert the previous observations that the key trigger of arrhythmia is activation of the cation non-selective channel and that interaction of K^+ channels with the non-selective SACs collectively contribute to the maintenance of arrhythmia. Figure 5 illustrates a case of mechanically induced sustained reentry at an interval of 140ms. In this case, after the impact is delivered, an action potential is generated below the impact zone which propagates through the posterior side of the ventricles (50 ms frame in Figure: 5). Activation of the reentrant cycle eventually encompasses both the ventricles (150ms and 290ms frames) and helps establish arrhythmia.

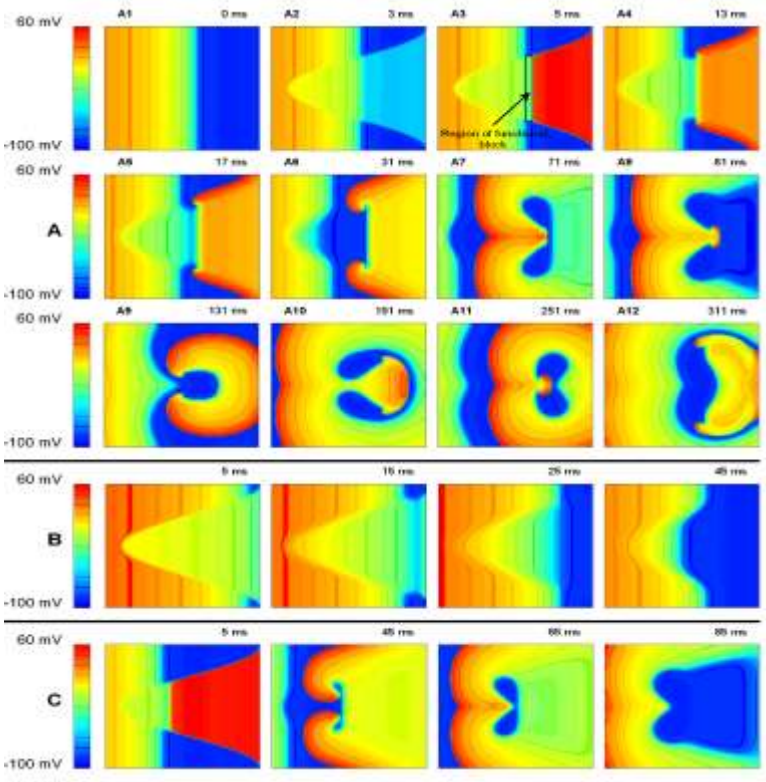


Figure 4: The 2D ventricular tissue slice model developed by Kohl et al (2004) in a 2.5 cm X 2.5 cm mesh. This model represents a slice through the ventricle free wall, with the endocardium to the left and the epicardium to the right. Panels A-C illustrates the different stages of tissue repolarization at different impact times (labeled as milliseconds-ms). Precordial impacts on cardiac tissue assume a bell-shaped force profile. (A) At 40% repolarization, the regionally differing effects of mechanically induced sustained arrhythmia. Frame A1 illustrates the timing of the impact. Frame A2 illustrates the subsequent activation of a cation non-selective SAC and partial repolarization of cells (tip of the force profile). Frame A3 illustrates suprathreshold depolarization between the wave end and the force profile base creating an ectopic focus (red color). The area labeled "Region of functional block" is the region where stretch-induced AP prolongation has occurred. Frames A4-A6 represents how the mechanically induced excitation can spread up or down and avoid the region of functional block. Frames A7-A12 represents the reentry of conduction pattern formed as a result of the generation of two oppositely oriented rotors of ectopic wavelets. (B) Early impact leads to 10% repolarization and lack of rhythmic disturbances. (C) Late impact (>60% repolarization) leads to a single ectopic beat. Figure adopted from Kohl & Garny, (2004).

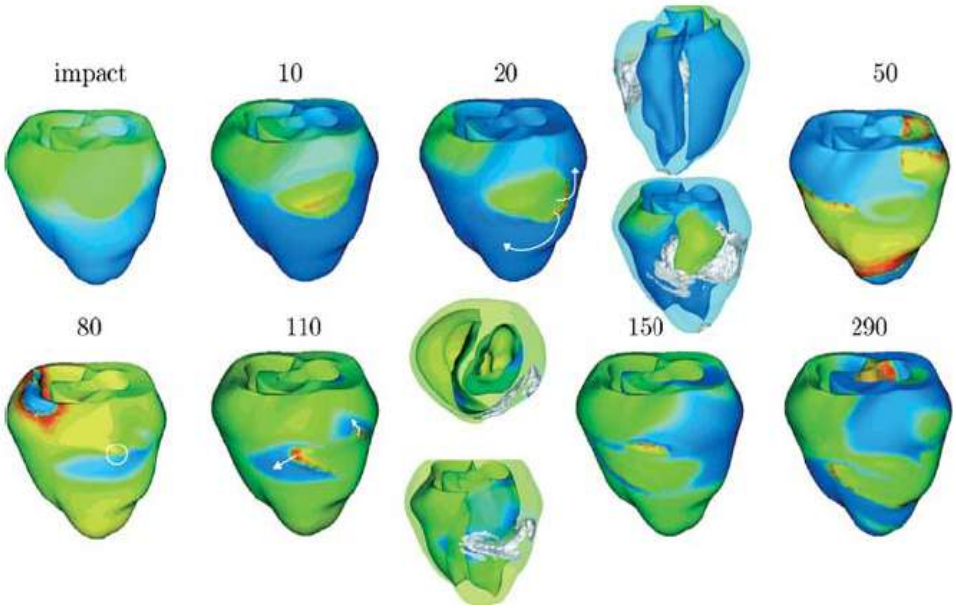


Figure 5: 3D Rabbit ventricular model developed by Li et al. (2004). This figure illustrates the evolution of transmembrane potential after a 140ms impact. The numbers above each image represent the time elapsed since the onset of the impact. The white arrows indicate the direction of propagation of the mechanically-induced wavefront. In the 80ms frame, the encircled region denotes the reentrant cycle traversing the original zone of impact. As shown, the wavefront propagates towards the apex and around the left ventricle and finally establishes arrhythmia in both the ventricles which subsequently culminates into ventricular fibrillation. The smaller images represent semi-transparent anterior, posterior and basal views of the ventricles depicted in the frames to their left. Figure adopted from Li et al. (2004).

Li and co-workers have identified several limitations with the rabbit ventricular model (Li et al. (2004)). For example, this approach failed to provide mechanistic details of how induction of reentry could be affected by the strength of an impact, nor does it take into consideration the contribution of space, time and amplitude on the activation of ion channels. While this model employs realistic fiber architecture, it does not take into account the heterogeneity associated with the ventricles, since this model assumes that all the cells have similar membrane properties (Li et al. (2004)). However, this model was indeed effective in providing a detailed view of the electrophysiology underlying arrhythmia following acute mechanical stimulation of the heart.

A 3D simulation of the ventricular free wall model depicted in Figure 4 was developed by the same investigators to assess whether the 2D findings were applicable in a 3D simulation. To test this, a 2.52 cm cube model was created in which a cylindrical shaped force profile was adopted (as opposed to the bell-shaped profile in the 2D simulation, Figure 4). This shape allowed for exclusion of time-dependent changes in the area of intersection with the repolarizing end (Figure 6). The results observed with this model were the same as seen with the 2D model. To summarize the findings with the 3D simulation: at 40% repolarization of the ventricular tissue, a mechanical stimulus applied at the peak of the T wave resulted in activation of stretch activated channels which determined the duration of the action potential. At this time-point, the mechanical impact created a scroll wave of ectopic excitation and sustained reentry (Frames 6-9 of Figure: 6). Thus certain key features of c*ommotio cordis* observed by experimental research can be reproduced in the ventricular models, the only discrepancy being the suggested role of cation non-selective stretch-activated channels as the key trigger underlying arrhythmogenesis (suggested by computational modeling) versus K^+ selective SACs suggested by *in vivo* cardiac models (Link et al. (1999)).

All the mathematical models described above provide useful insights about the electrophysiological behavior associated with cardiac arrhythmias. The 2D and 3D models reviewed above however provide no insights into the mechanism of gating and cell membrane dynamics associated with mechanically-induced arrhythmias. Also these mathematical models are computationally costly and intensive. Increasing the complexity of the model makes it more

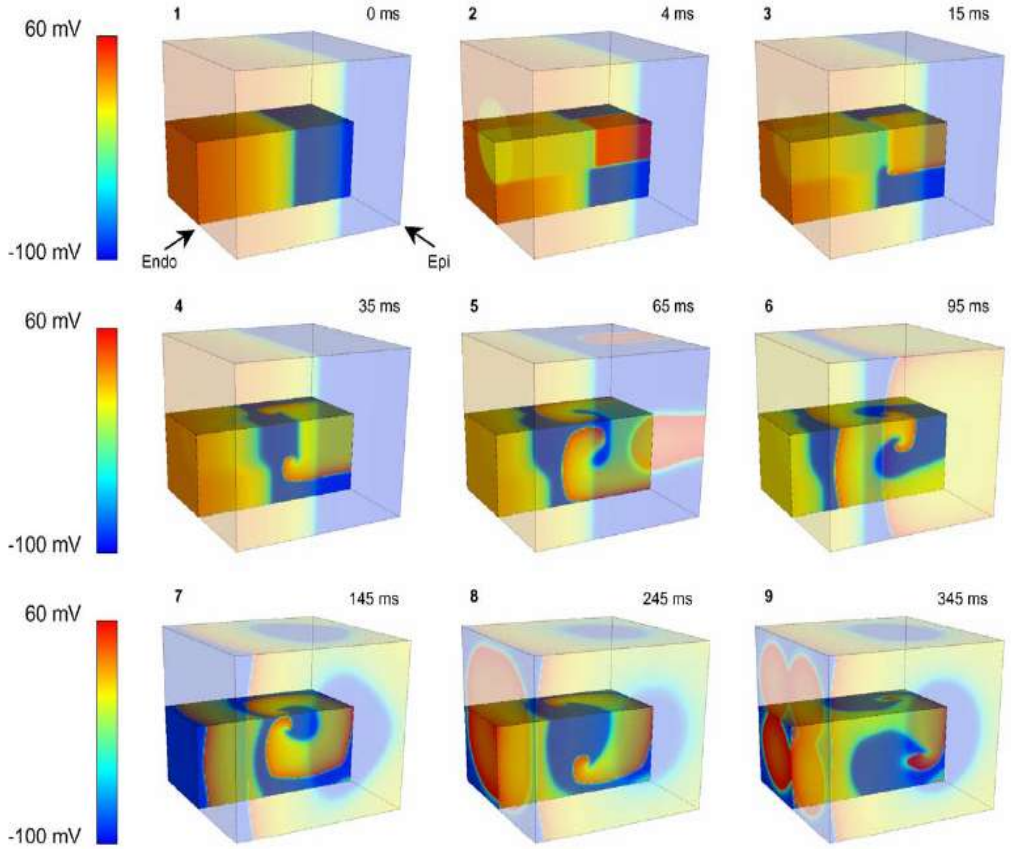


Figure 6: 3D ventricular free wall model developed by Garny et al. This figure illustrates the sustained arrhythmia following a mechanically induced stimulation in the early T-wave window. The force profile in this figure is a cylinder with a diameter of 1.26 cm. This figure again illustrates the region of functional block as the triggering factor for arrhythmogenesis. Figure adopted from Garny et al. (2005).

difficult to analyze, validate and interpret (Garny et al, (2005)). For this reason, finite element systems are much more suitable and adaptable to complex models and can represent the complexity in greater details.

CHAPTER III Finite Element Modelling of Gated Mechanosensitive Channels

3.1 Continuum-based Simulations and Mechanobiology

Continuum mechanics simulations in the finite element framework have been widely used in the biomechanical field to study systems with complex geometries such as the dynamics of lipids and membrane proteins (Wang et al. (1998); Phillips et al. (2002); Zumdieck et al. (2005); Bathe, (2008)), ion channels (Tang et al. (2006, 2008)) and even transport systems. This method is favored over other analytical methods mentioned above (such as all-atom simulations, target and equilibrium molecular dynamic simulations, etc), since finite element models allow for the introduction of complex membrane deformations over multiple time and length scales, thus enabling a much more realistic representation of biomolecules and their assemblies. Thus the finite element method (FEM) is more accessible to studying the conformational response of mechanosensitive (MS) channels to external mechanical perturbations in the membrane (Tang et al. (2006)). Tang and co-workers are pioneers in the field of FEM simulations in studying gating transitions in mechanosensitive channels. Their work has mainly focused on gating transitions in the bacterial MS channels of *E.coli* and *M.tuberculosis*. In a cellular environment, MS channels are subjected to a range of mechanical stimuli acting on the membrane (or its associated components), including high-frequency vibrations, shear stress due to fluids, hemodynamic and hydrostatic pressures, osmotic pressure gradients and steady-state contractions. In response to these stimuli, MS channels change their conductive state via conformational changes. To simulate how these conformational transitions are regulated in response to mechanical stimuli, Tang and coworkers (2006) used the FEM analysis to incorporate different deformation modes into the cell membrane and observe the corresponding response of the MS channel. Deformation modes fall into two broad categories: In-plane distortions (stretching and shearing) and out-of-plane distortions (bending and twisting). In order to simulate mechanotransduction in a more realistic manner, it is imperative to take into consideration the complex stress fields surrounding the MS channels that are initiated as a result of the different deformations acting on the cell membrane. These considerations are outside the scope of conventional MD simulations and more

importantly, remote loads that indirectly influence MS channel gating, cannot be modeled using MD simulations (Tang et al. (2006)).

FEM simulations can be applied to study gating in other mechanosensitive channels such as the transient-receptor potential channels that mediate auditory transduction in *Drosophila* (Kernan, (2007)) and other voltage-gated channels such as the *Shaker* potassium channel. The versatile nature of the FEM model makes it accessible to studying other complex membrane-mediated biomechanical processes such as cardiac arrhythmias, muscle contractions, cytokinesis and maybe even touch and hearing.

3.2 Gating Mechanism of the Mechanosensitive Channel of Large Conductance (MscL): Insights from Continuum-based FEM Simulations Developed by Tang and coworkers

The following is a brief account of the model developed by Tang and coworkers.

3.2.1 The FEM Model

E.coli or *M.tuberculosis* MscL are usually used as model systems (Tang et al. 2008; Sukharev,2004) to study gating transition mechanisms of MS channels because of its simple structure and ubiquitous nature. Figure 7 illustrates the continuum model of *E.coli* MscL (*Ec*MscL) developed by Tang et al. (2008). Each helix is modeled as an elastic rod (of 55Å in diameter) embedded into a homogenous elastic membrane. The transmembrane 1 (TM1) helices form the inner pore of the channel and make limited contact with the phospholipid membrane, whereas the TM2 helices interact extensively with the lipid membrane forming the outer boundary of the channel. For this model, the helix is considered homogenous and isotropic thus rendering the elastic properties constant throughout the gating transition. Relevant material properties of the TM helices, such as the Young's modulus and Poisson's ratio, were adopted from Sun et al (2005).

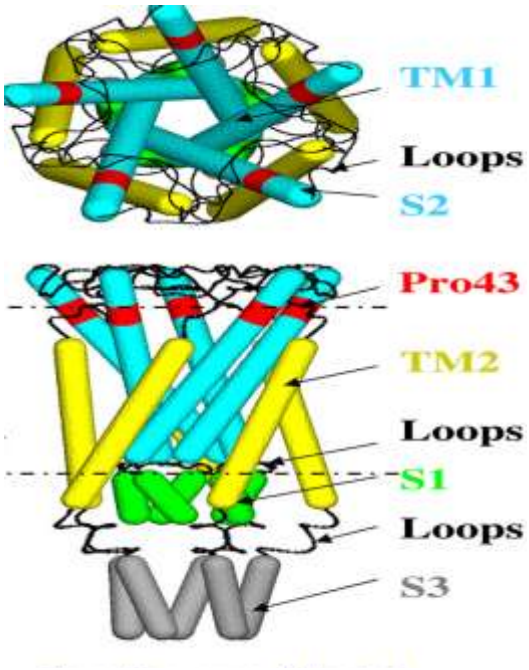


Figure 7: Top and side view of the closed state of the *E.coli* MS channel FEM model. The dashed line represents the lipid bi-layer membrane and the different helices are labeled as S1 and S3 (cytoplasmic helices), TM1 and TM2 (transmembrane helices) connected through cytoplasmic and periplasmic loops. S2 is the segment above the Pro43 break in the TM1 helix. (Figure from: Tang et al. (2008)).

The lipid bilayer in this model was modeled as a 35 A° thick elastic sheet with no distinctions made between the head and tails of the phospholipid (Figure 8). For this simulation study, Tang and coworkers only applied equi-biaxial membrane tension and axisymmetric bending to the membrane and studied the response of MscL. However, other large-scale deformation modes and complex mechanistic perturbations too are accessible to this model (Tang et al., (2008)). The size of the membrane employed in this simulation was 400 X 400Å and the Young's modulus was estimated from the area compressibility.

The interaction between the transmembrane helices and between the helices and the lipid bilayer in this model was assumed to obey an effective pair-wise potential function similar to the Lennard-Jones form:

$$E_{\text{int}}(\alpha)=C\left[\frac{n}{m}\left(\frac{d_0}{\alpha}\right)^m-\left(\frac{d_0}{\alpha}\right)^n\right]. \quad \text{(Tang et al., (2008))}$$

Where $E_{int}\ (\alpha)$ is the effective interaction between the surfaces of either of the two components described above. d_0 and α are the initial equilibrium distance and deformed distance between the two surfaces and m and n denote the power indices for the repulsive and attractive terms where $n<m$ (Tang et al., (2008)).

3.2.2 Gating Mechanism of MscL

3.2.2.1 MscL Gating upon Equi-biaxial Tension

Upon application of an equi-biaxial strain of 21% to the lipid membrane, the lipid cavity expanded (as depicted in Figure 9) and transmitted the forces to the TM helices via non-bonded interactions, which subsequently led to the opening of the TM1-enclosed pore. With this model, the TM1 was found to bend more than the TM2 helices and this was necessary in order to maintain mechanical equilibrium throughout the gating process (Tang et al. (2008)). Much of the

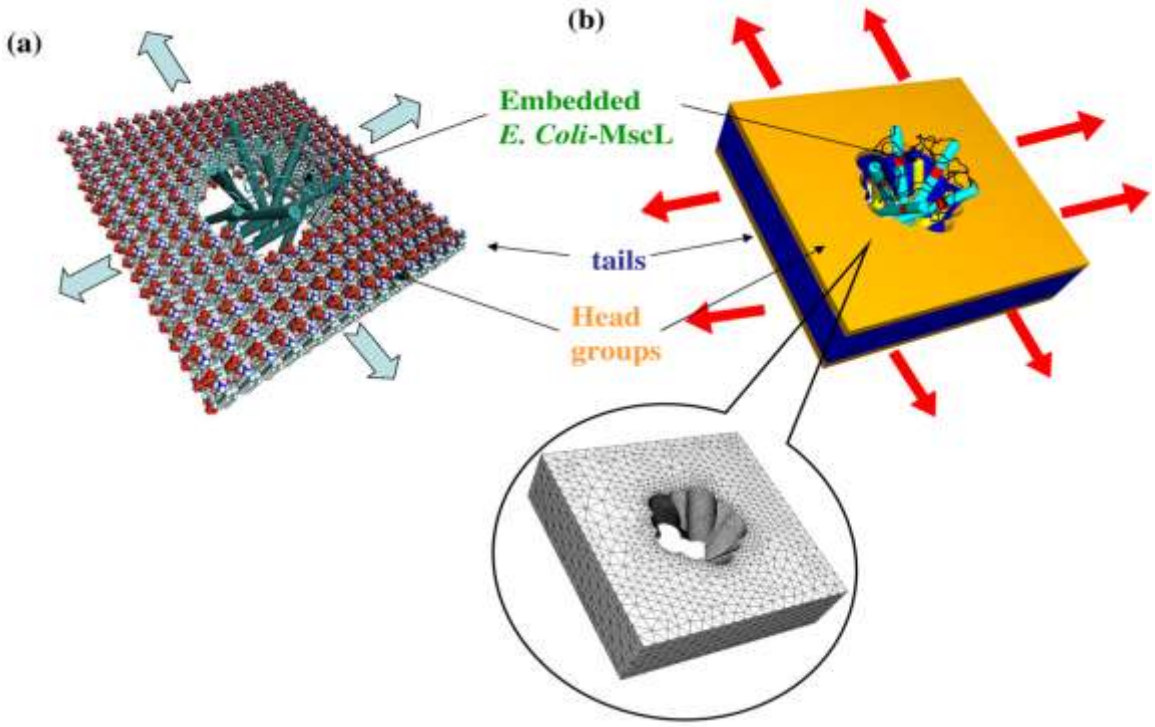


Figure 8: (a) The finite element mesh for the lipid bilayer membrane embedded with *E.coli* MscL during equi-biaxial tension. (b) The assembled continuum structure of an *E.coli* MscL inside a lipid bilayer. The inset illustrates the cavity created to accommodate the MscL. Figure adopted from Tang et al. (2008).

conformational changes observed during gating with the FEM model were in conformation with previous structural models of *E.coli* MscL (Sukharev et al. (2004)). For example, during gating, the S1 helix was found to expand radially, in a "swing-like motion", towards the transmembrane region, while the S3 helix remained unchanged. Even the increment of the pore radius was in agreement with previous steered MD simulations (Gullingsrud & Schulten, (2003)). However, a few deviations from previous simulations were observed. For instance, the free energy profile differed significantly from previous simulation studies and the channel pore radius essentially remained constant when different types of tension were applied to the membrane. But it is believed that these deviations could be resolved if the FEM model took into consideration the effect of solvation forces on membrane dynamics (Tang et al. (2008)).

3.2.2.2 MscL Gating upon Bending

Bending was not effective in gating the MscL channel, since the radius of the channel pore did not change significantly with bending moment. If bending was coupled with in-plane deformations, then the protein would probably undergo conformational changes, but bending alone was not sufficient to open the channel pore (Figure 10).

3.2.2.3 Contribution of the Structural Motifs to MscL Gating

When individual structural motifs that comprise the MscL channel are removed, the contribution of each group to mechanotransduction and more specifically to gating can be individually assessed. To that end, when the periplasmic loops that connect the TM1 and TM2 helices were cut the TM1 tilting angle decreased by 10° and altered the shape of the S1 and S3 helices. This suggests that the loops have a role to play during the gating process. Similarly when the SI/TM1 linker loops are removed, the constraining effect decreases and opens the channel pore much wider. On the other hand, removal of the S3 bundle had no significant effect on any of the transmembrane protein components (Tang et al. (2008)). All these findings were consistent with experimental observations made on MscL gating (Anishkin et al. (2003); Sukharev, Durell & Guy, (2001)) and highlight the importance of the individual structural motifs in regulating gating. Figure 11 illustrates the effect of individual protein structural motifs on gating.

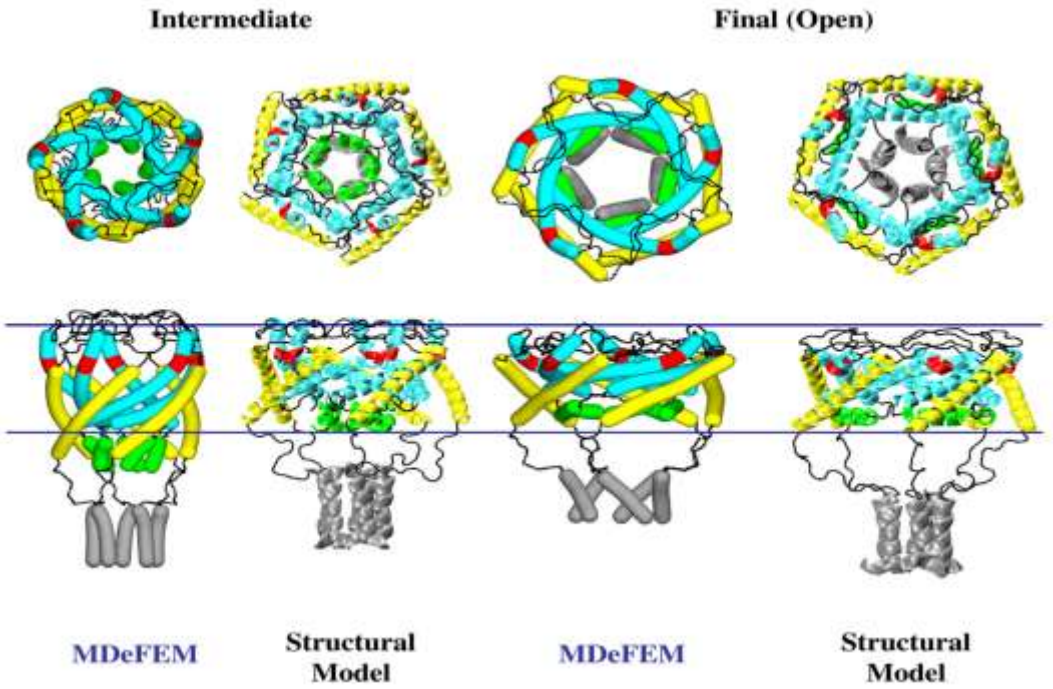


Figure 9: Comparison of the gating transition pathway of MscL obtained by the structural model developed by Sukharev et al and the FEM model developed by Tang et al. The first two panels illustrate the half-opened state of the channel upon application of an equi-biaxial tension and the last two panels illustrate the fully-opened state. The protein (TM) helices interact with the lipid layer via non-bonded interactions and mediate the radial expansion of the transmembrane helices and the subsequent opening of the TM1 bundle. Figure adopted from Tang et al. (2008).

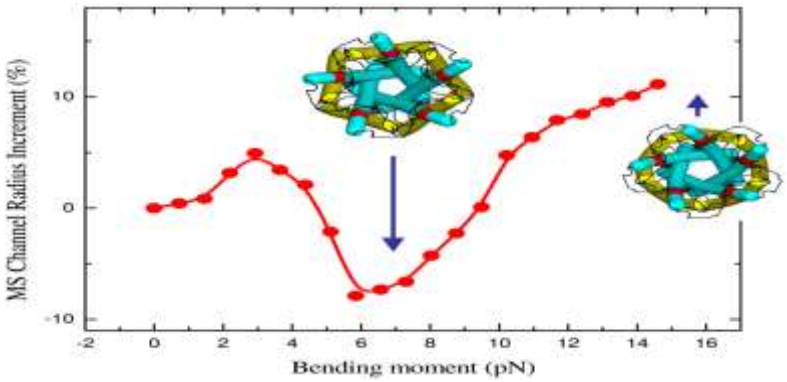


Figure 10: Pure bending of the membrane does not increase the radius of the channel pore significantly. Even though the protein undergoes a conformational change, the pore radius does not enlarge enough to promote gating. Figure adopted from Tang et al. (2008).

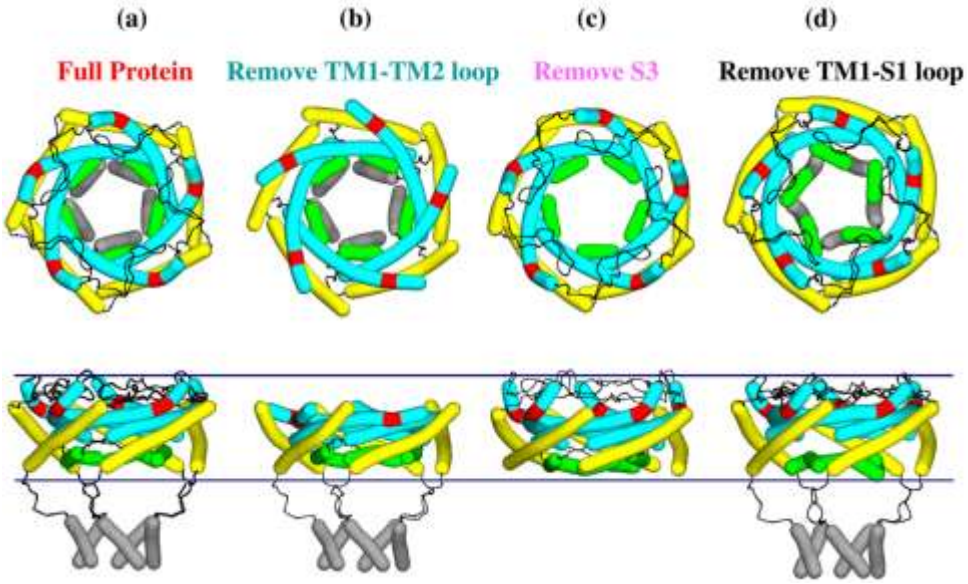


Figure 11: Effects of removing structural components of the MscL channel on gating behaviour. Panel 1 represents the full protein without any structural motifs cut. In panel 2, the TM1-TM2 loop is removed and this altered the shape of the S1 and S3 helices. In panel 3, the S3 helix bundle is removed, no change in conformation of the protein is seen. In panel 4, the TM1-S1 loop is removed and this leads to a distortion of the S1 pore. Figure adopted from Tang et al. (2008).

CHAPTER IV FEM Modeling of TbMscL using Autodesk® AutoCAD 2007 & ABAQUS®

The previous chapter dealt with providing a general insight to the field of Finite Element Modeling in analyzing a mechanosensitive channel. The current chapter gives an in-depth account of the modeling process, structural assumptions and features. Autodesk® AutoCAD 2007 was used for the construction of the model. This model was then imported to ABAQUS® (v6.5) and Finite Element Analysis was performed on it.

4.1 The Geometry

As has been previously mentioned, the structures that contribute in the gating mechanism of an MscL are the protein that makes up the channel and the surrounding lipid membrane. It is postulated that the lipid membrane's mechanical properties have the maximum effect on the gating mechanism of the channel. The protein consists of different types of transmembrane helices (TM) that are arranged together in a specific array as demonstrated in Figure 12. The equivalent CAD models that have been created for the current study are also illustrated in Figure 12 (c), and (d). It can be observed that the structural model is more closely packed than the FEM model. This does not result in any significant error as the main idea is to check for the change in the structure and not overall increase in length. The surrounding structures of this assembly consist of connecting loops and cytoplasmic TMs that are ignored as can be seen from the structural model; these structures are not included in the FEM model to reduce the complexity of the model. However, future models that incorporate these structures are bound to get more accurate results and will be helpful in furthering our understanding of these channels. Detailed structural description of the channel will be discussed later on in the chapter.

The lipid membrane surrounding the channel has a prominent role to play in the gating mechanism of the channel as the material properties of the membrane affect the gating behavior of the channel. As we are considering a single channel and a small slice of the surrounding lipid

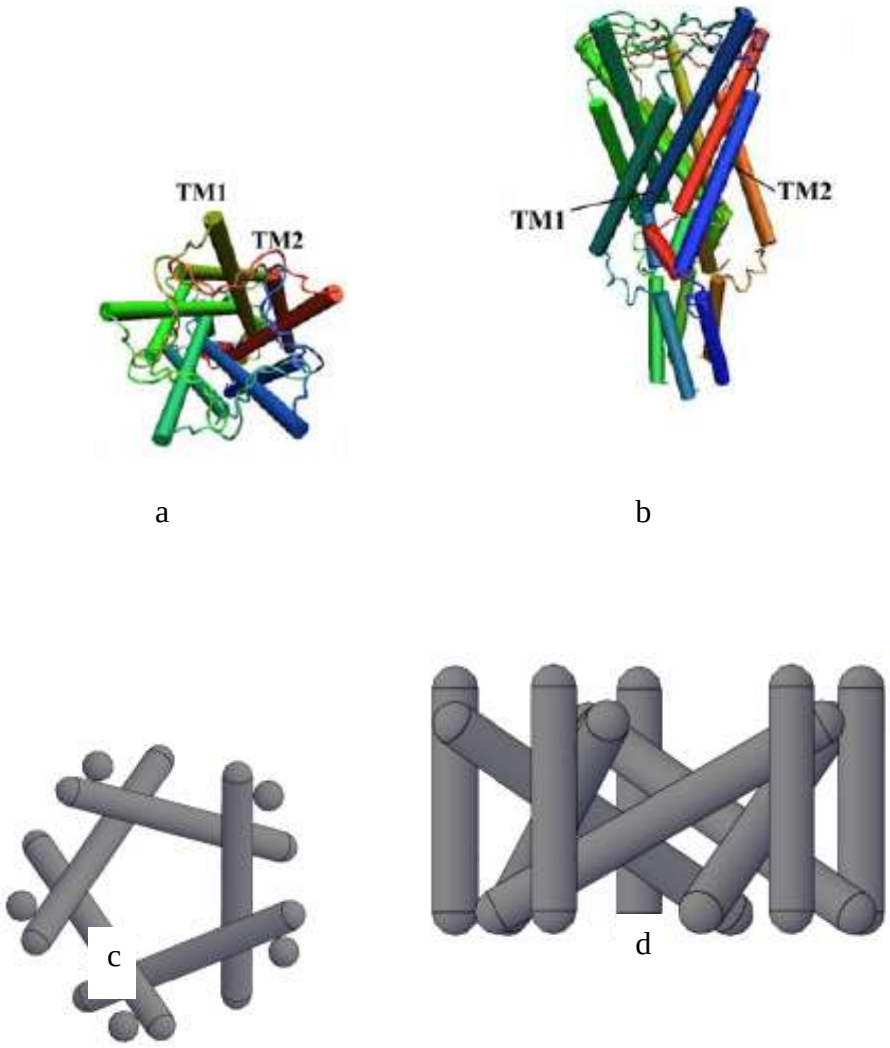


Figure 12: Structural and Finite Element model of the channel. (a, b) Top and side structural views of the channel (c, d) Top and side views of equivalent FEM model. Figures (a) and (b) have been adopted from Tang et al. (2006).

membrane, it can be assumed that the lipid membrane has a planar structure with homogenous properties. Detailed structural description of the layer will be dealt with later on. However, this is just an assumption, in reality the structure varies with depth and improvements of the current model are discussed in the future directions chapter.

4.2 The Helices

As was discussed earlier, only two transmembrane helices; TM1 and TM2 were considered in the FEM model. The material properties of the transmembrane helices have been adapted from Tang et al. (2006). In this model, both the helices are modeled as elastic rods that have homogenous and isotropic mechanical properties.

4.2.1 TM1 & TM2 Helices

Transmembrane helix TM1 is the longer of the two helices. The height of the cylinder representing the helix was modeled to be 42Aº with a radius of 5Aº. It should be noted that this is a simplified model of the helix and features like the break in the helix due to the residue Pro-43 (Tang et al. (2006)) have been ignored.

Transmembrane helix TM2 is shorter than TM1 helix. The level of interaction between TM2 helix and the lipid membrane is high. Also, in this model the helix is partly embedded into the lipid membrane. Tang et al. (2006) had formed a petal like structure to embed the helix. However, significantly similar results were observed between their model and the current model. A schematic difference between the dimensions of the two helices can be observed in Figure 13. The helices are made uniform without taking into consideration any Lennard-Jones interaction potentials. This potential develops due to the interaction of the hydrophobic and hydrophilic ends of the helices. However, for simplicity this has been ignored. The other major difference in the current model is that the split in the helices due to Pro-43 has been ignored for simplicity.

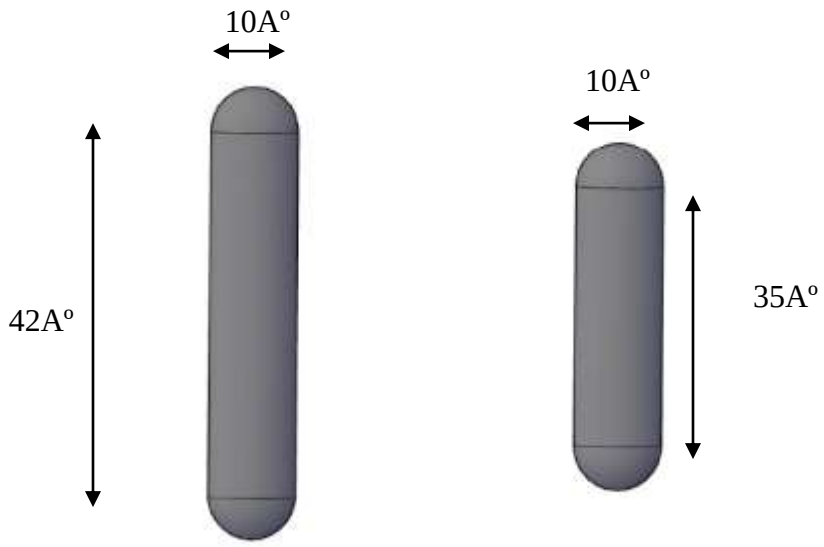


Figure 13: 3D CAD models of TM1 and TM2 helices with their dimensions.

As has been mentioned before, the helices have been modeled with spherical end caps, this has a two-fold effect on the structure, firstly, it helps create a structure without any hard/sharp corners and secondly, it helps in the convergence of results. The TM1 and TM2 helices have a varied level of interaction through the length of their structures, however to maintain simplicity the two helices are bonded as can be seen in Figure 14. Although in the earlier models of the channel proteins, TM1 and TM2 helices are inclined with the normal (the Out-of-plane axis), the current analysis models the TM2 helix parallel and the TM1 helix makes an angle of 45º to the normal.

Lets us consider a TM1-TM2 combine arranged as discussed in the previous paragraph as a single unit. The channel then is made of five such units having five TM1 helices and five TM2 helices, respectively. The polygon that the top view of the channel forms is a cyclic pentagon. One important parameter that often is measured for checking the state of a channel is the radius of the channel and the next section discusses this important parameter.

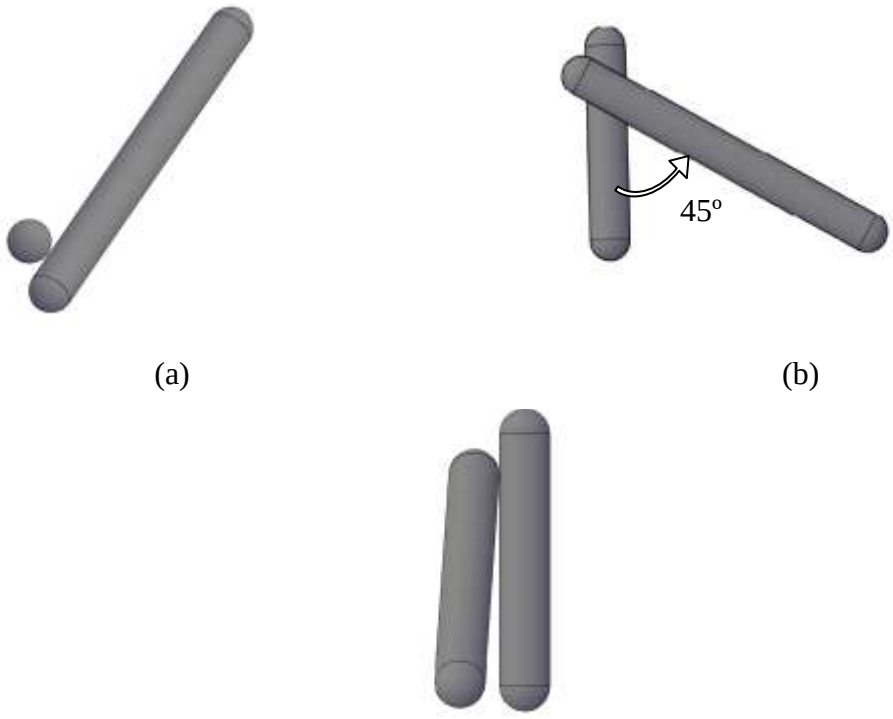


Figure 14: 3D views of the TM1-TM2 helix combine. (a), (b) and (c) show the top view, side view and front view of the combine respectively.

The material properties of the helices are mentioned in the meshing section. A summary of the geometrical properties of the helices are mentioned in Table 1.

4.2.2 Radius of the Channel

The radius of the channel is defined as the maximum radius of the cylinder that can be inscribed in the inner gap of the channel. For the current study the channel is modeled with a radius of 11Aº. The radius of the channel is the single most important parameter of study in this analysis, as it determines the state of the channel. Figure: 15 illustrates the concept of the radius of the channel by placing a hypothetical cylinder in between the helices and the radius of the cylinder represents the radius of the channel.

4.3 The Membrane

As has been mentioned earlier, the stress distribution in the lipid membrane surrounding the channel due to stretching is the primary cause of the channel's gating process. The surrounding channel is vast and for the current analysis, a cubical section, 400Aº (L) x 400Aº (B) x 35Aº (H), around the channel was assumed as the membrane. The membrane has a hole with a radius of 22Aº at its center to house the channel. The material properties of the membrane are mentioned in the meshing section. For the current analysis, the membrane is considered to be homogenous and isotropic. However, for future analysis increasing the complexity will make the model more accurate and this will be discussed in the future directions section. Figure 16 illustrates the model

Table 1: Summary of Geometric Properties of the Helices

Property	**Value**	
	TM1 Helix	**TM2 Helix**
Height	42Aº	35Aº
Radius of Spherical Cap	5Aº	5Aº

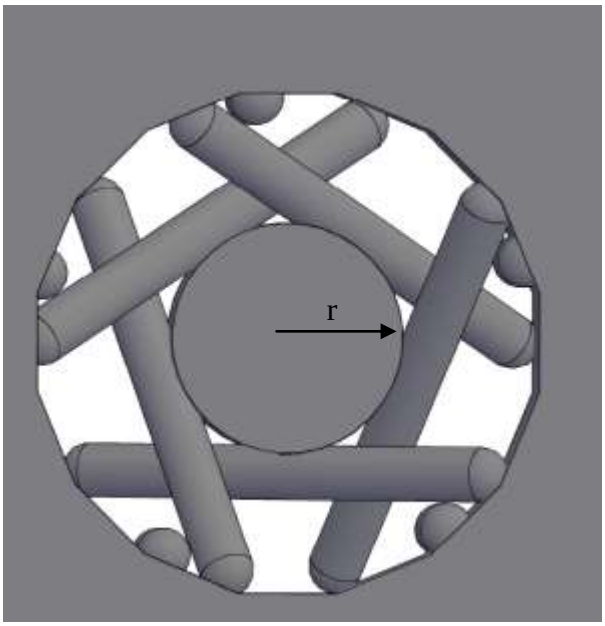


Figure 15: The Radius of the Channel; the current figure depicts a hypothetical cylinder with radius ‘r’ that represents the radius of the channel.

of the membrane constructed for the current analysis. The geometric properties of the model are mentioned in Table 2.

4.4 The Membrane-channel Combine

The TM2 helices of the channel are partly embedded into the membrane creating two contact points between the helix TM1 and the membrane. Figure 17 illustrates the channel-membrane integration. It can be observed that one end of the channel is relatively close to the top of the membrane, this was done because of the fact that the channel starts at the surface of the membrane and extends into the cell body.

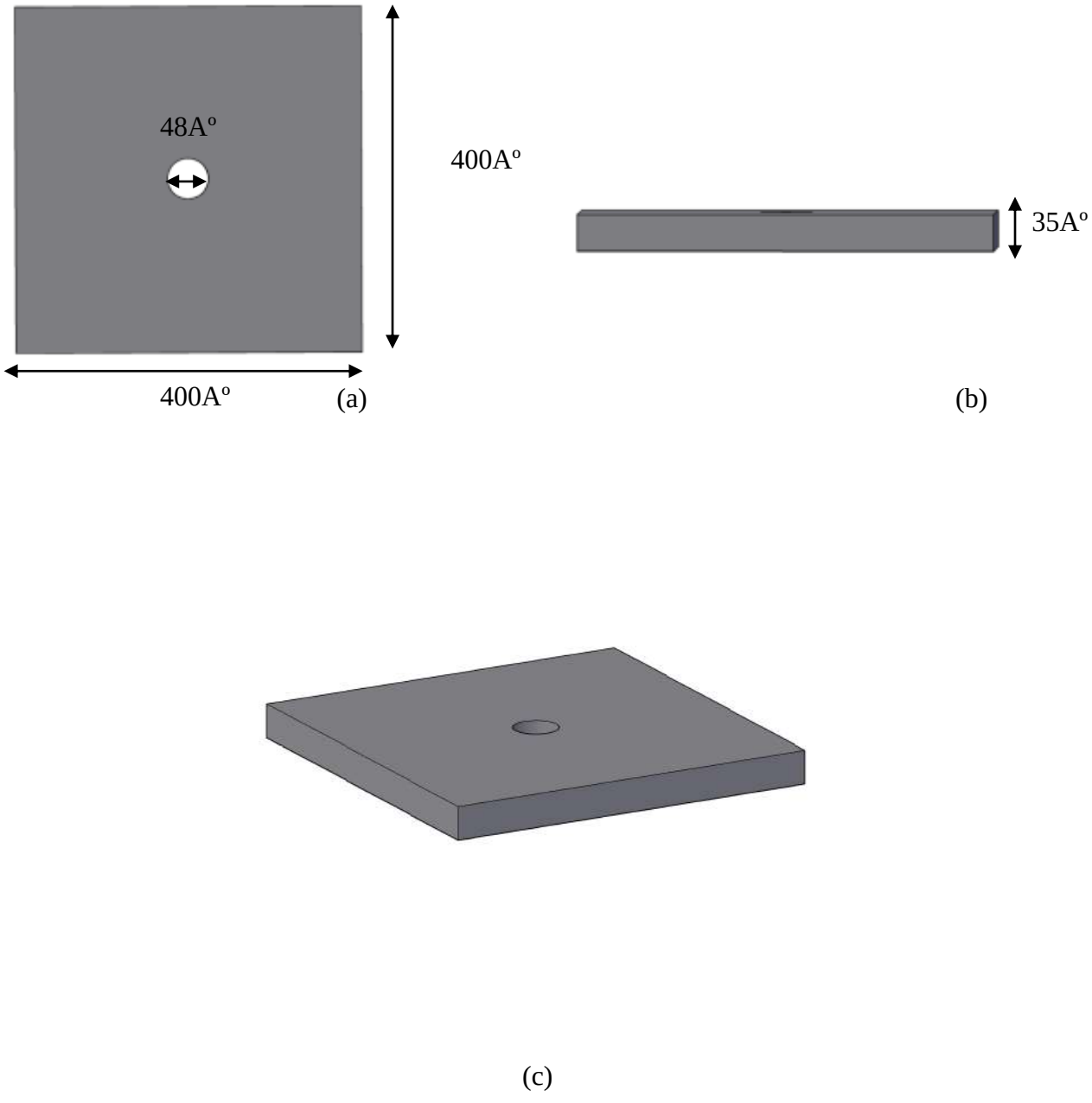
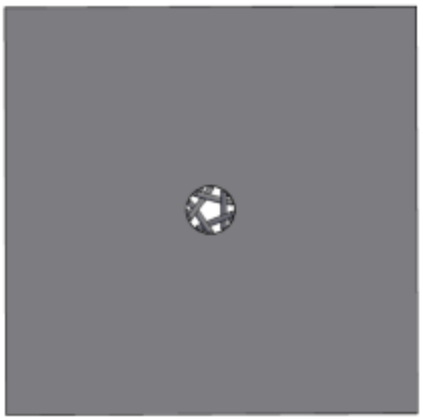


Figure 16: (a) and (b) represent 2D views of the membrane with the dimensions. (c) represents the 3D view of the structure.

Table 2: Geometric Properties of the Membrane Model

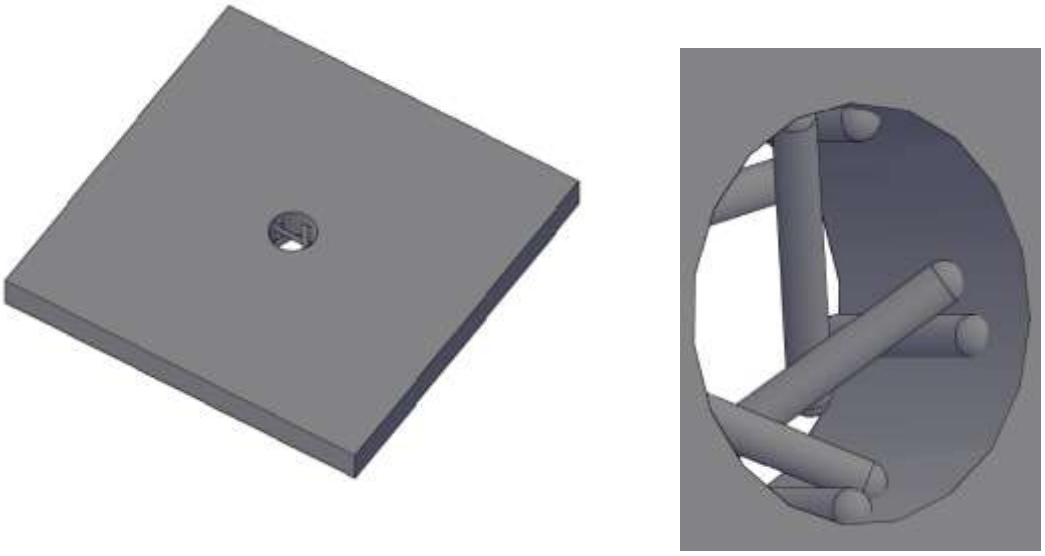
Property	**Value**
Length	400Aº
Wdith	400Aº
Thickness	35Aº
Radius of the Hole	48Aº



(a)



(b)



(c) (d)

Figure 17: The Membrane-channel combine. (a), (b), (c) represent the different geometric views of the model. (d) gives a closer look at the TM2 helix-membrane integration.

4.5 The Two-channel Membrane-channel Model

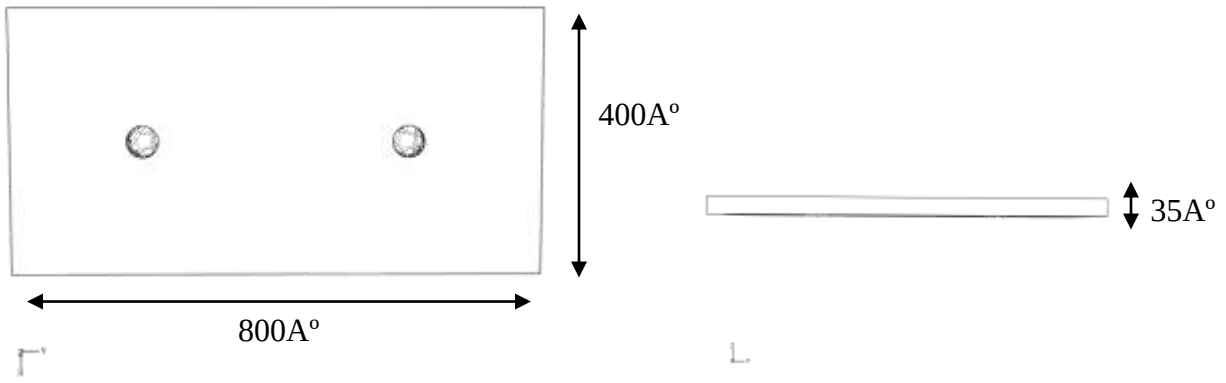
The two-channel membrane-channel model is an extension of the single-channel model. In this model, two single channels were joined together at one edge and the analysis was performed on it. Figure 18 shows a two-channel membrane-channel model. Figure 18 (a) & (b) represent the 2D cross-sectional views of the two-channel model with the dimensions of the model highlighted.

4.6 The Heart

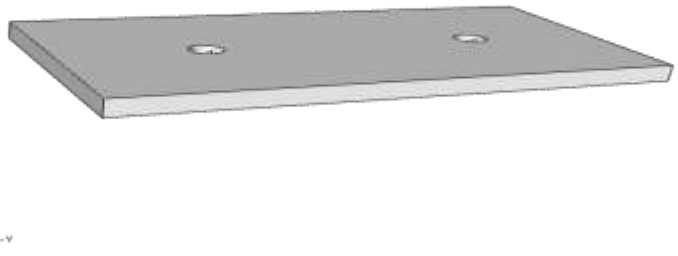
To study *commotio cordis* using the membrane-channel model, the stress on the heart's surface due to a blow had to be computed. To achieve this, a 3D model of the heart was studied to check its stress response. The model is an open-source model developed by **Michael Barenboym** and was imported from 3DContentCentral.com. The model can be found at: www.3dcontentcentral.com/downloadmodel.aspx?catalogid=171&id=4453. The model is an accurate representation of the normal human heart (Figure: 19).

4.7 Meshing

This section describes the meshing process employed for the membrane-channel model and the heart model. As has been mentioned earlier, the models were created in Autodesk® AutoCAD 2007 and then were exported in the *.sat format (ACIS SAT file) into ABAQUS®. The membrane-channel model was imported as a solid; however, the heart model was imported as a shell. The following is a brief discussion of the meshing process for both the models.



(a) (b)



(c)

Figure 18: (a), (b) represent the dimensions of the two-channel model in 2D. (c) represents a 3D view.

Table 3: Geometric Properties of the Two-channel Membrane Model

Property	Value
Length	800Aº
Wdith	400Aº
Thickness	35Aº
Radius of the Holes	48Aº

4.7.1 Membrane-Channel Model

As mentioned earlier, this model (figure 19) was imported as a solid structure into ABAQUS®. The complete model was defined as an elastic material. Different features of the model were assigned properties based on the study by Tang et al. (2006) and is mentioned in Table 4.

A global element size of five is selected for the model as an element size more than five causes the creation of unusable elements. Free tetrahedral mesh was implemented in meshing the model, the boundaries, however, were assigned mapped meshing controls. The number of elements formed with these settings is **306382** with **59792** nodes. As the global size is small, the number

of elements and nodes created are large and thus the computation time taken for carrying the analysis is greatly increased.

4.7.2 Two-channel Membrane Model

The two channel membrane is the second step in the current analysis. This was designed to quantify the behavior of the channel in the presence of another channel. It was modeled by joining two membrane-channel models. So, the dimensions of this model are 800Aº (l) x 400Aº (b) x 35Aº (h). The material properties of this model were assigned similar to the single channel model. A global element size of 20 is selected for the model. Free tetrahedral mesh was implemented in meshing the model, however, the boundaries were assigned mapped meshing controls. The number of elements formed with these settings is **38449** with **9595** nodes.

4.7.3 The Heart

The heart 3D model was imported as a shell into ABAQUS®. As the model is complex, the global element size of 0.03 was assigned to the model. Although, the elements that were formed after the mesh were small and represented the model well, there were still some structural anomalies in the model. These unusable elements were found around the aorta and the arc of aorta. As the analysis dealt with obtaining the stress profile around the atria and ventricles, the upper features of the heart were partially ignored. Figure 22 shows the difference between the actual model and the meshed model.

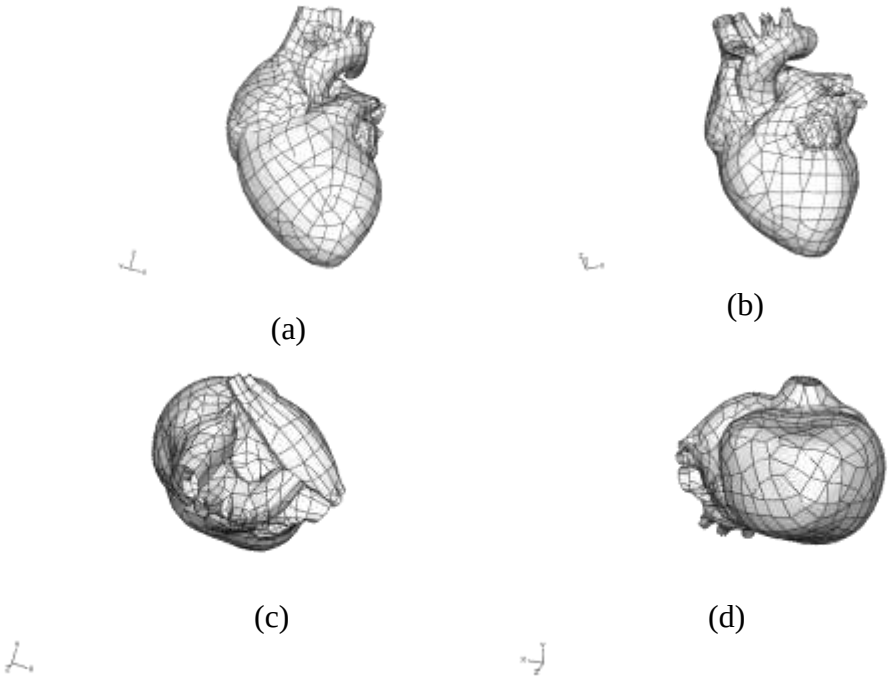


Figure 19: Different views of the heart model. (a) posterior view, (b) anterior view, (c) top view and (d) bottom view.

Table 4: Material Properties of the Features of the Membrane–channel Model.

Feature	Young's Modulus	Poisson's Ratio
Membrane	0.1 GPa	0.3
Channel (TM1 helix)	100 GPa	0.3
Channel (TM2 helix)	100 GPa	0.3

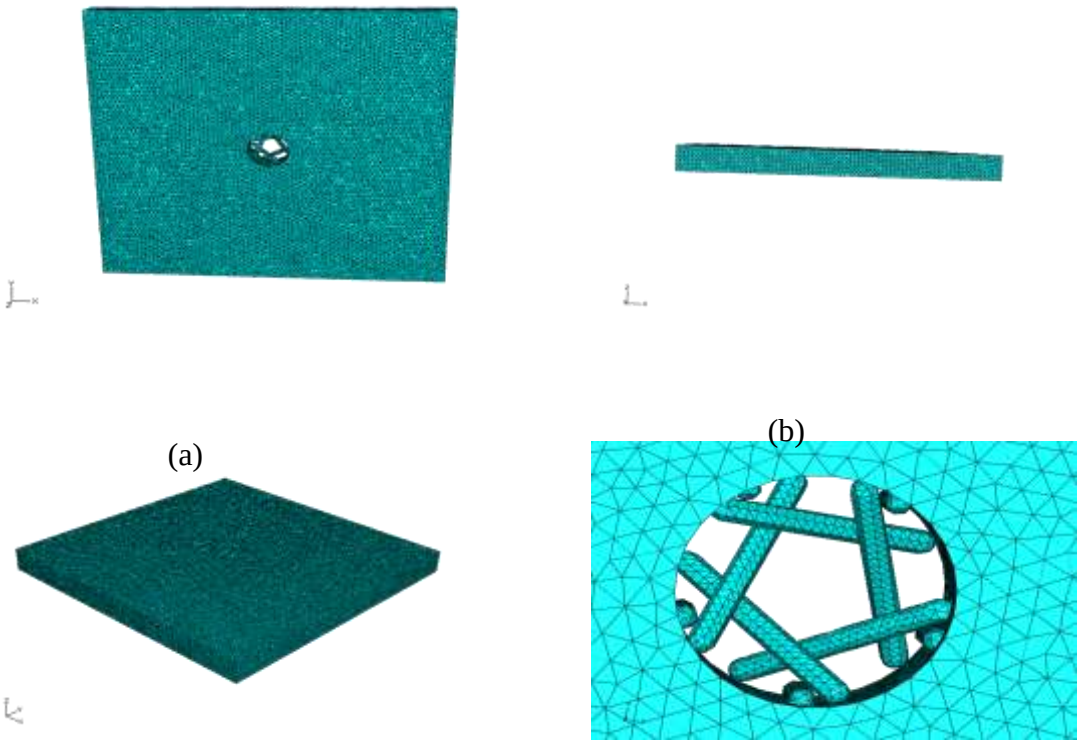


Figure 20: Membrane-channel model mesh. (a), (b) and (c) respectively, illustrate 2D front, side and 3D cross view of the meshed combine. (d) demonstrates the visual of the mesh profile around the channel.

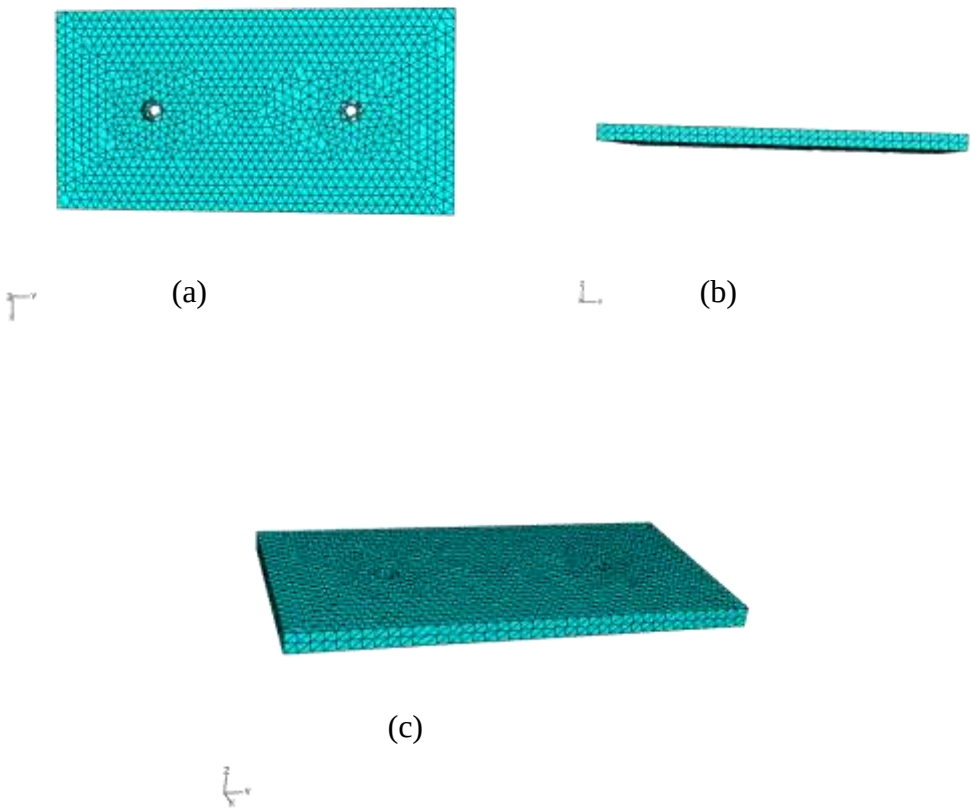
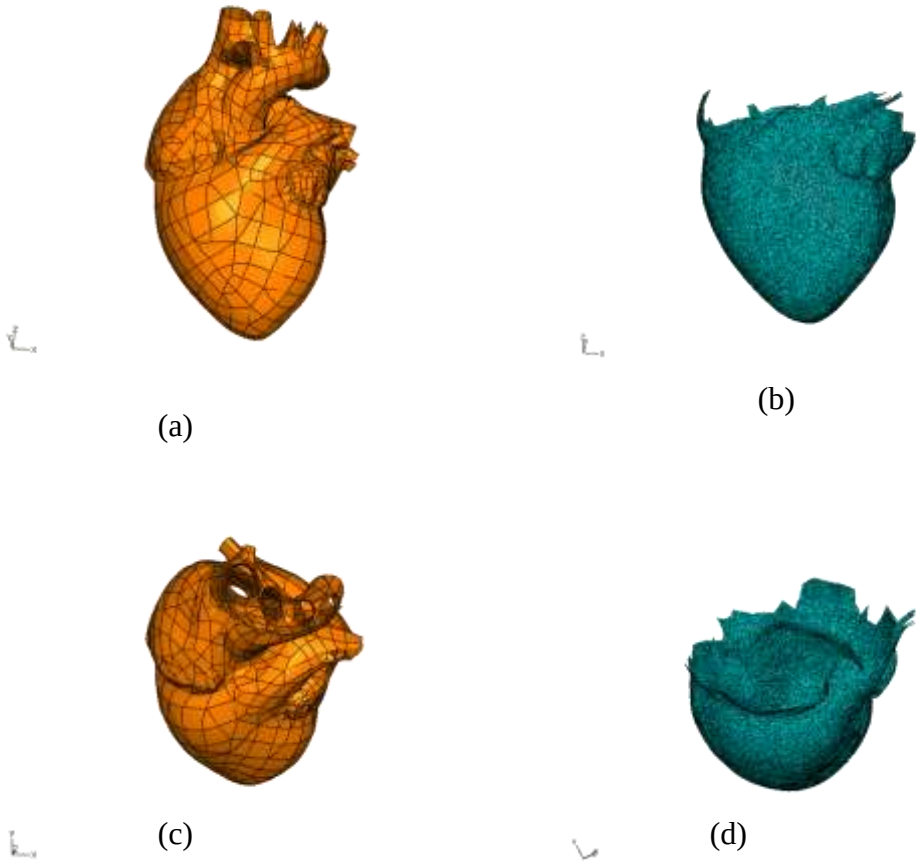


Figure 21: Membrane - two-channel model mesh. (a), (b) and (c) respectively, illustrate 2D front, side and 3D cross view of the meshed combine.



(a) (b)

(c) (d)

Figure 22: Pre and Post mesh views of the heart model. (a) anterior view before the mesh, (b) anterior view after the mesh, (c) top view before the mesh and (d) top view after the mesh.

Table 5: Differences in the Properties of the Actual and the Modified Heart Model.

Feature	Actual Model	Modified Model
Young's Modulus	1 GPa	1 GPa
Poisson's Ratio	0.045	0.045
No. of Nodes	-	72861
No. of Elements	-	73367

CHAPTER V Results

This chapter describes the actual steps in the analysis, the different loading coditions applied and the results obtained. The analysis was performed on a Pentium D 3.2GHz processor, 2GB RAM computer running Windows® XP SP3 operating system. The time taken for meshing and carrying out the analysis was about 1.5 h. The membrane-channel model was subjected to in-plane stretching and out-of-plane bending. The heart model on the other hand was just subjected to in-plane stretching.

5.1 Membrane-channel Model

After the model was imported into ABAQUS® and meshed, the next step in the analysis involved applying boundary conditions and subjecting the model to various loads. The loads applied were based on the model developed by Tang et al. (2006) in which they had computed the maximum in-plane load to be close to 35 MPa, an estimate that they concluded will cause the channel to open completely. The boundary conditions applied were mainly to curb rigid body motion as the model was a solid.

5.1.1 Boundary Condition

5.1.1.1 In-plane Stretching

In-plane stretch does not require any specific initial boundary condition as bi-axial tension is applied on the four sides of the structure. However, as the structure is to be deformed in two dimensions, all out-of plane deformations were blocked by restricting displacement and rotation in the Z-direction of the model. Figure 23 illustrates this condition. As can be observed, the XY plane represents the plane of the membrane.

5.1.1.2 In-plane stretching - Two-channel Model

This model has similar boundary conditions as the original membrane-channel model. Here all the nodes have restricted Z direction displacement to ensure that there are no out-of-plane events. Figure 24 illustrates the boundary conditions being applied to the two-channel model.

5.1.1.3 Out-of-plane Bending

The out-of-plane bending was achieved by restricting two nodes that were diametrically opposite on the edge of the hole on the membrane. The nodes were not pinned (no degrees of freedom), but could not have any displacement in the direction of bending. The nodes were randomly chosen and do not adhere to any earlier study. Although the bending test was performed by applying a bending force both in the positive and the negative direction, the boundary conditions were not altered. The same nodes were restricted for both the tests. Figure 25 depicts the boundary condition applied for the out-of-plane bending test.

5.1.1.4 Out-of-plane Bending - Two-channel Model

Four nodes were restricted in this model in the Z-direction. Two nodes each were selected from the diametrically opposite edges of the two holes. Figure 26 illustrates these features.

5.1.2 The Loads

5.1.2.1 In-plane Stretch

As has been mentioned earlier, the loads used in this analysis are synonymous to the loads used by Tang et al. (2006) in their study. They had postulated that a maximum load of 35 MPa was enough to open the channel completely. The load was applied bi-axially around the membrane and thus rigid body motion also was eliminated. The load was set to increase linearly over the

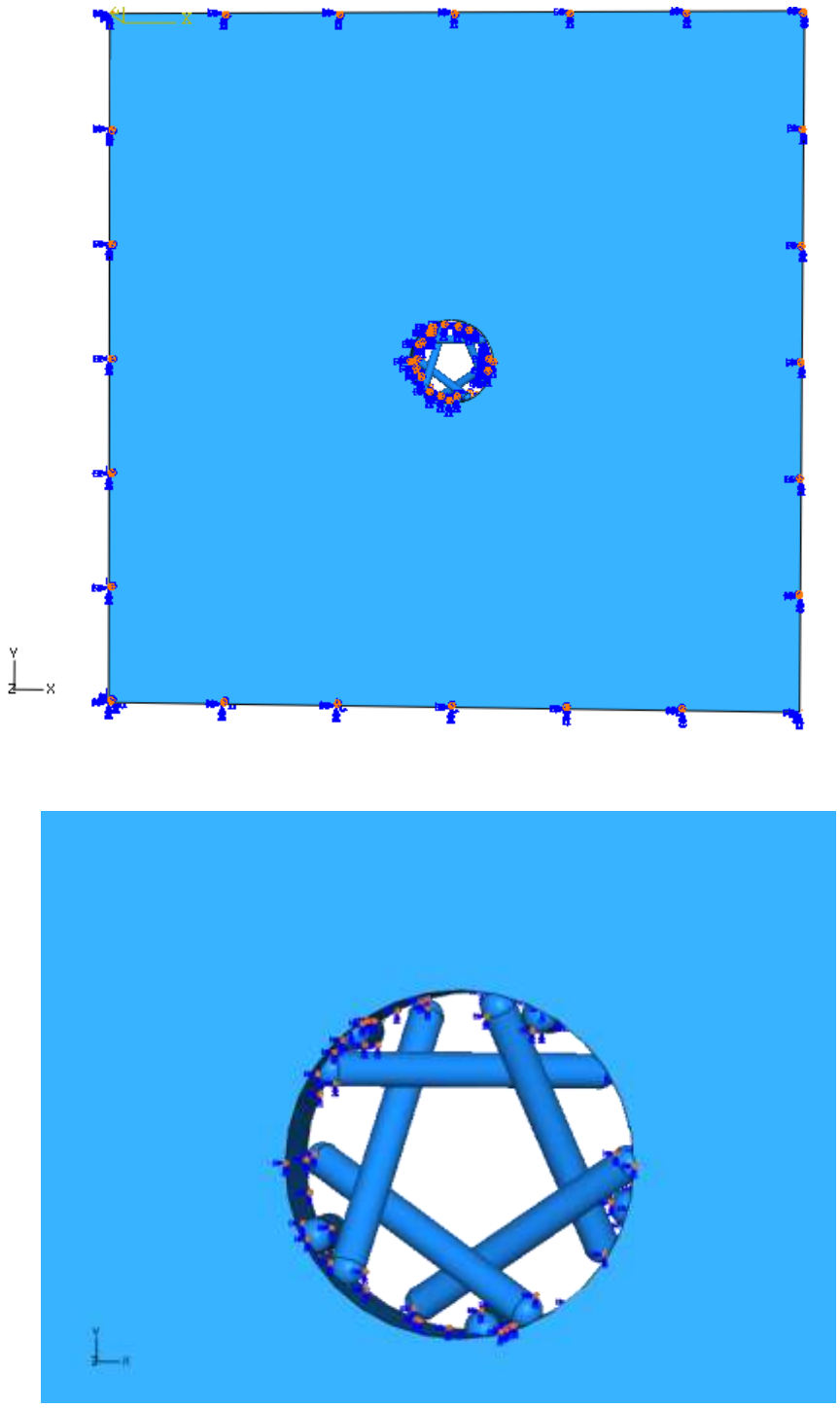


Figure 23: Boundary conditions applied for the in-plane stretch mode on the membrane-channel model.

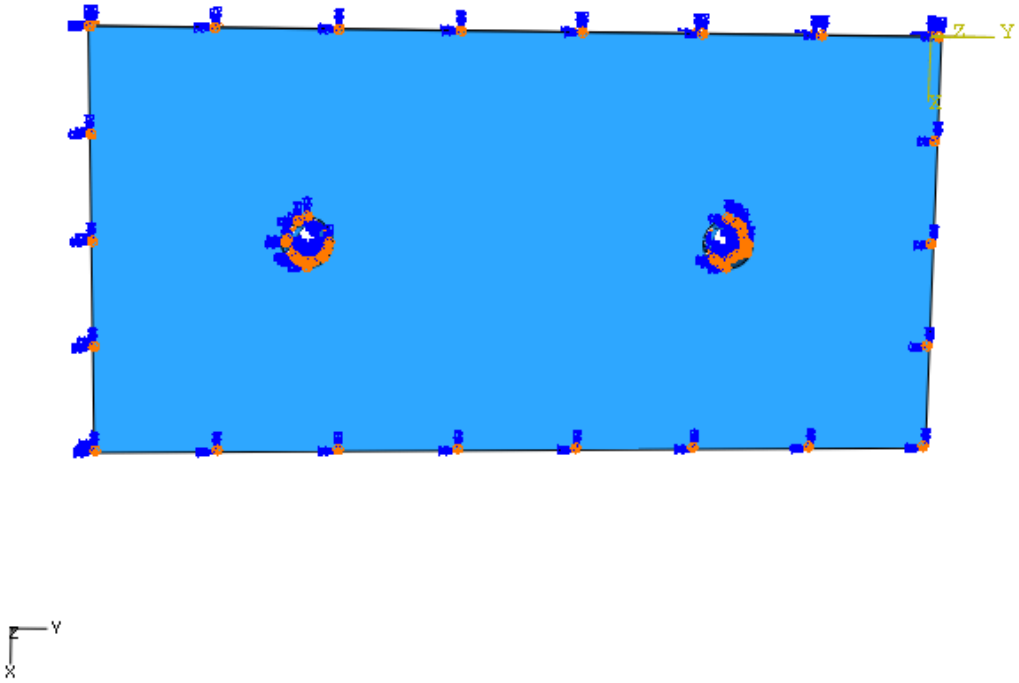


Figure 24: Boundary conditions for the in-plane stretch mode of the two-channel model.

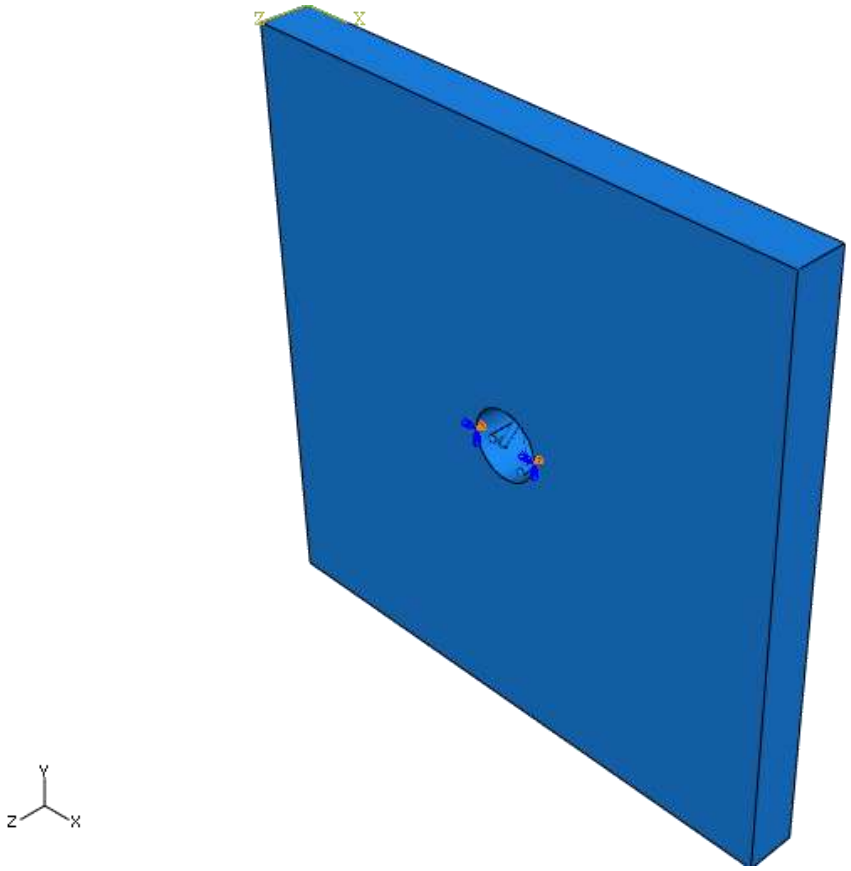


Figure 25: Out-of-plane bending deformation applied on the membrane channel model

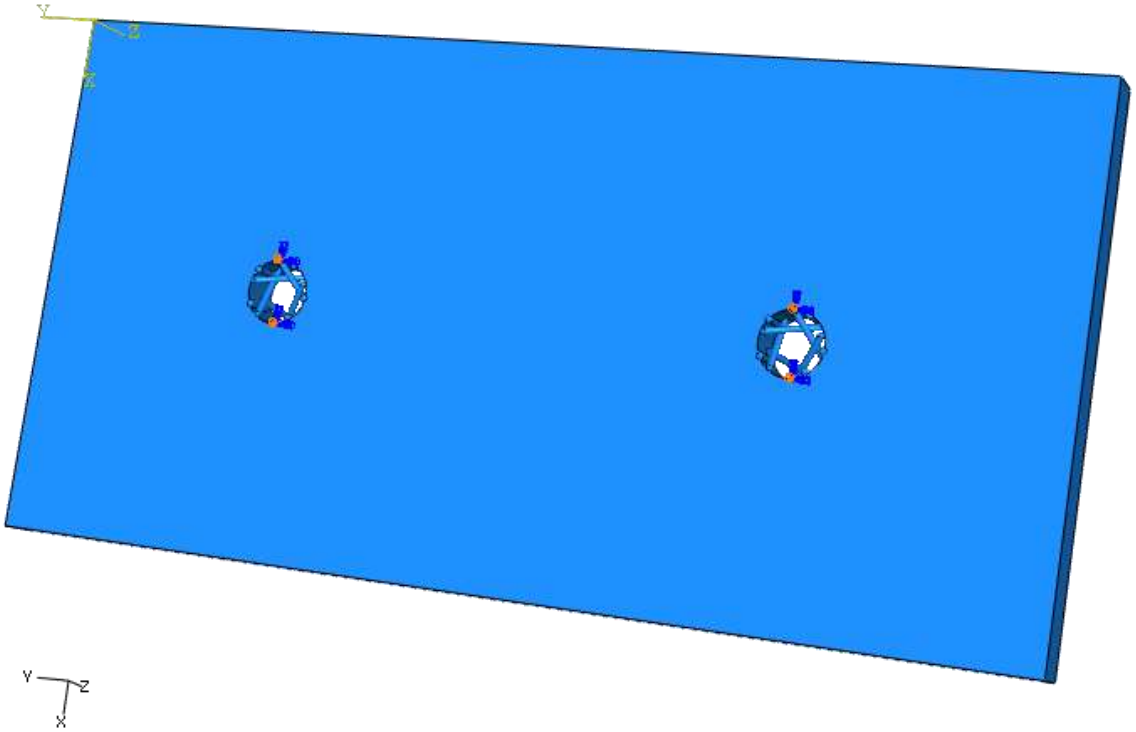


Figure 26: Out-of-plane bending deformation applied on the two-channel model.

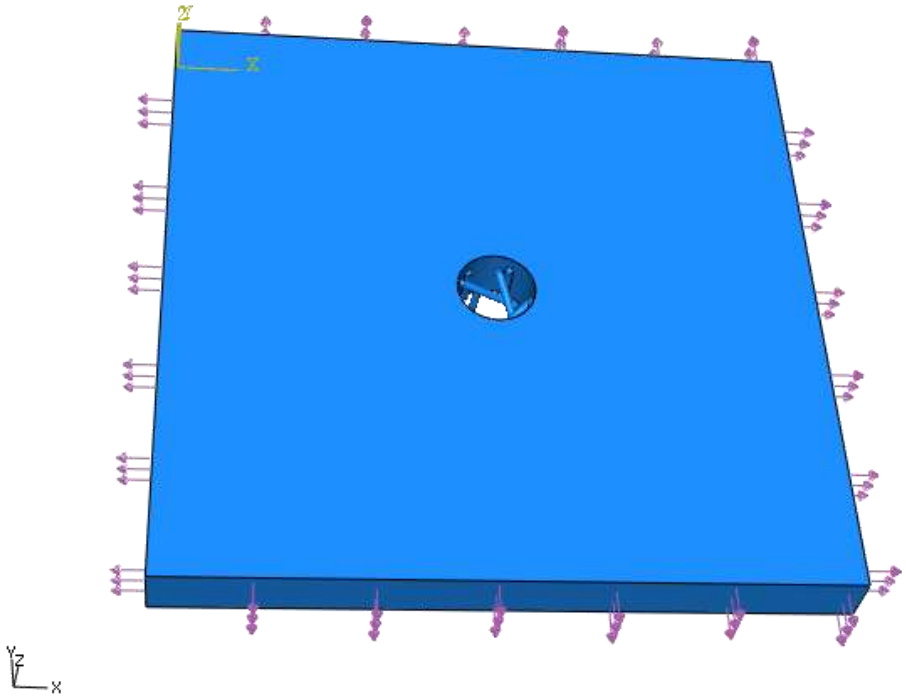


Figure 27: Force applied to the outer edge of the membrane. The magnitude of the force is 35MPa. It increases exponentially from 0 to the maximum load over the time period of the simulation.

As mentioned in chapter I of this thesis, there are very few models that deal with multi-channel analysis. Thus, as there is insufficient data on multi-channel models, the current analysis was performed by applying the same in-plane tension as in the single-channel model i.e. 35 MPa. Figure 28 illustrates the two-channel model with the tension applied to the edges.

Axisymmetric bending was applied to the membrane-channel model to simulate the effects of bending on the channel. Tang et al. (2006) in their study had calculated the moment to bend a circular disc with radius 200 Aº to be ~1800 pNnm. For the current model the bending force applied was calculated as:

$$\text{Bending Force} = (1800\ \text{pNnm})/(1600\text{Aº}) \sim 0.125\ \text{pN}$$

This bending force was then applied to the model at the edges. This can be observed in Figure 29. For bending, the force is applied in both the positive and negative Z-direction to check the channel's response. Figure 29 shows the force being applied in the positive Z-direction.

5.1.2.4 Out-of-plane Bending - Two-channel Model

The load on the two- channel model is calculated by the same method as the single-channel. The bending force thus obtained for the two channel system was 0.15 pN. This was applied at the four edges of the membrane. Figure 30 illustrates the application of bending force on the two channel membrane. The force was applied both in the positive and negative Z-direction and the current plot illustrates the application of force in the negative Z-direction.

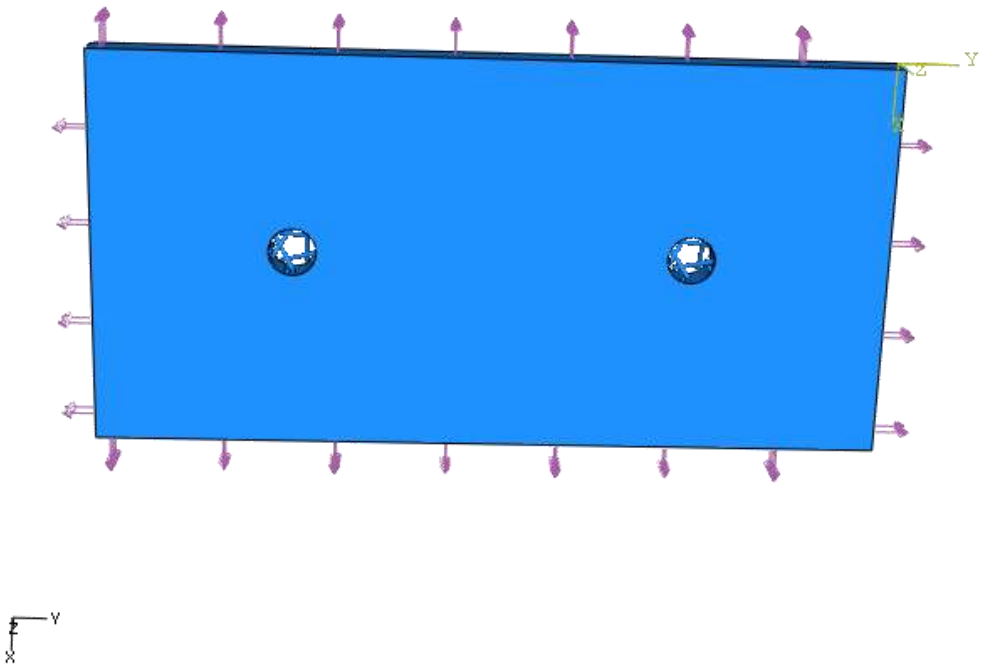


Figure 28: In-plane bending deformation of 35 MPa applied to the two-channel model.

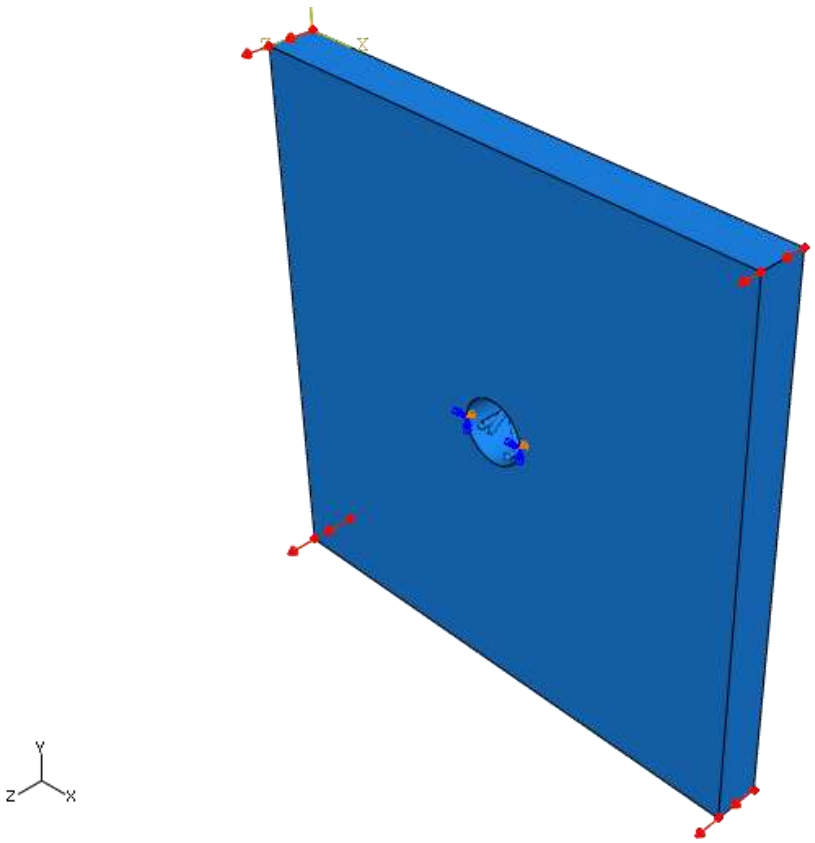


Figure 29: Out-of-plane bending applied to the membrane channel model in the positive and negative Z-direction.

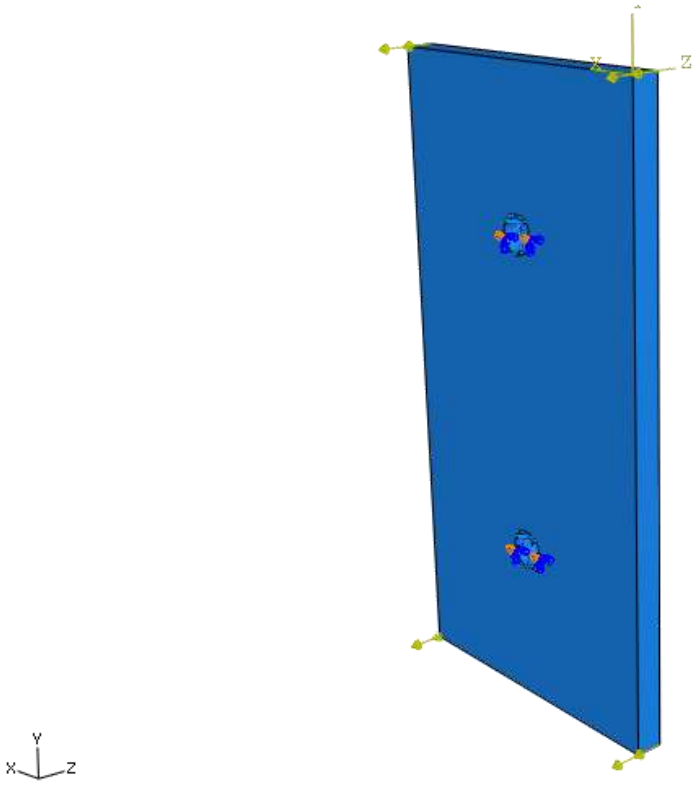


Figure 30: Out-of-plane bending deformation applied on the two-channel model.

5.1.3 Results of the Analysis

The current section deals with the detailed results obtained after the loads and boundary conditions mentioned previously were applied on the models. This section lists all the results of the analysis and the discussion on these results will be provided in the next section. The order of the results is:

(i) In-plane stretch

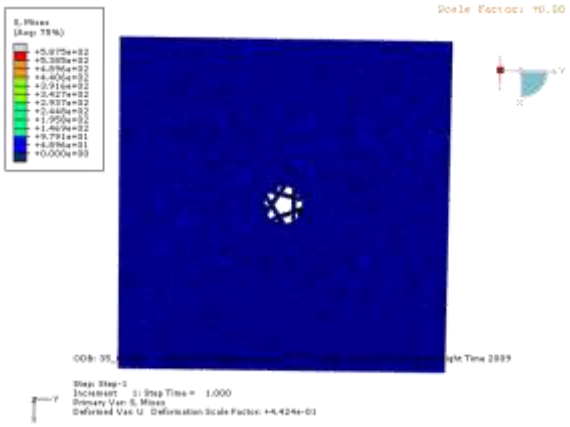
(ii) In-plane stretch- two-channel

(iii) Out-of-plane Bending

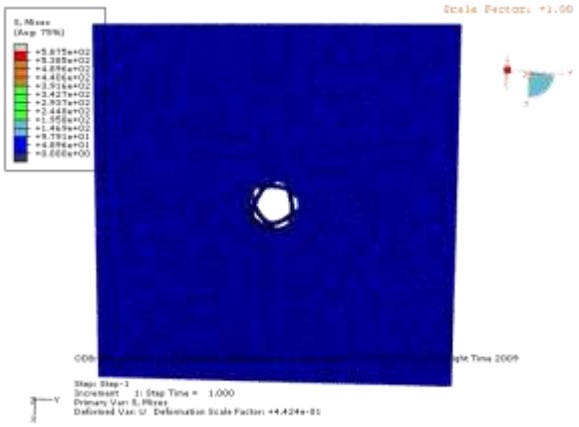
(iv) Out-of-plane Bending – two-channel

5.1.3.1 In-plane Stretch

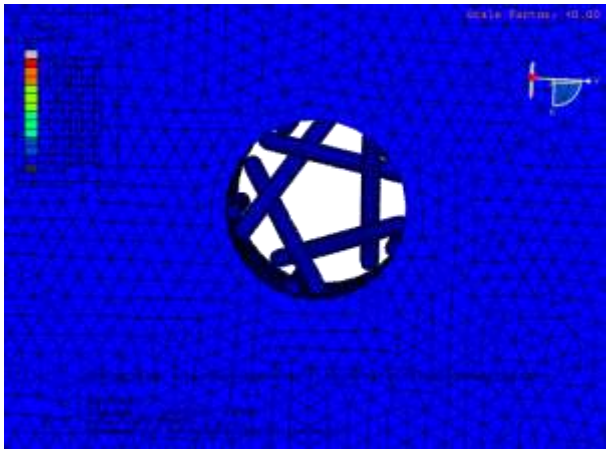
As has been discussed in the previous section, an in-plane stress of the magnitude of 35 MPa was applied on the edges of the membrane uniformly. This load was designed to gradually increase from to 0 to 35 MPa over the time period of the simulation. This was done in order to observe the geometrical transition happening within the channel and the membrane. The time period of the simulation was set to 1sec and 7 frames were established to check the transition of the results. The frames represent results at t = 0, 0.14, 0.29, 0.43, 0.57, 0.71, 0.86, 1 s. Table 6 following the frames presents the change in diameter of the hole and the channel. As was discussed earlier, the radius of the channel is the most important variable measured to study the gating mechanism of a channel; the change in diameter of the various structures is mentioned after the pictorial results. The nodes mentioned in the results are the nodes that are diametrically opposite each other. The first two images in Figure 31 show the beginning and the end states of the Membrane-Channel model.



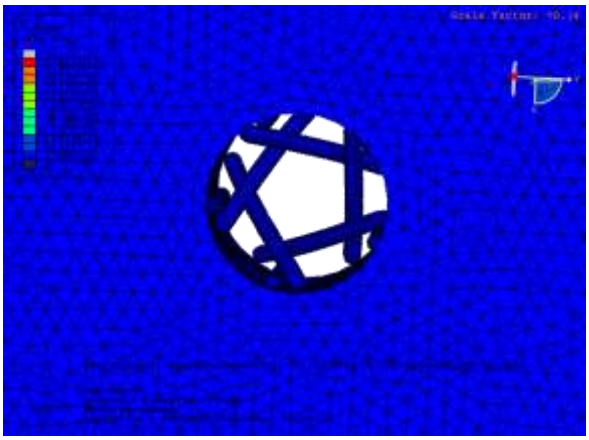
Initial State



End State

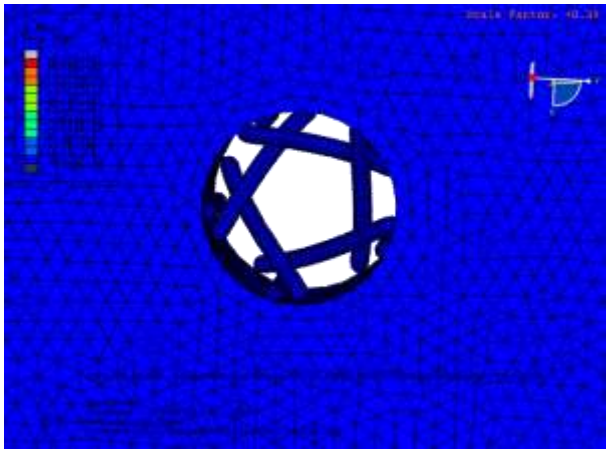


t=0

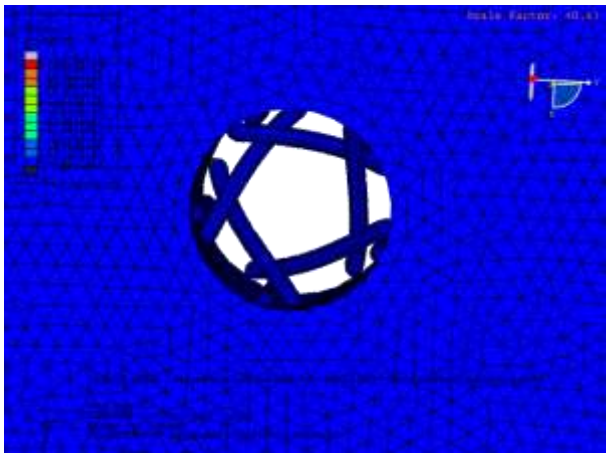


t=0.14

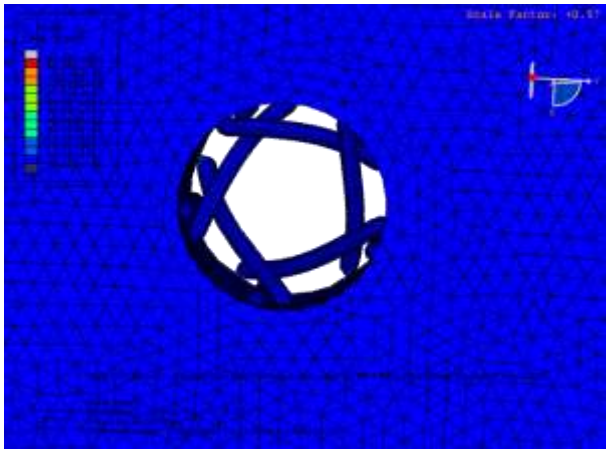
Figure 31



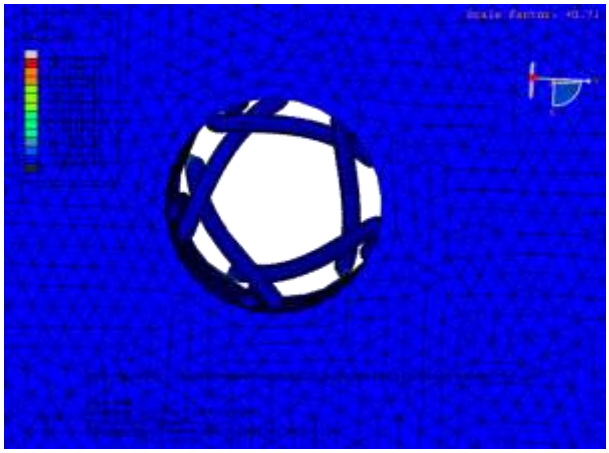
t=0.29



t=0.43

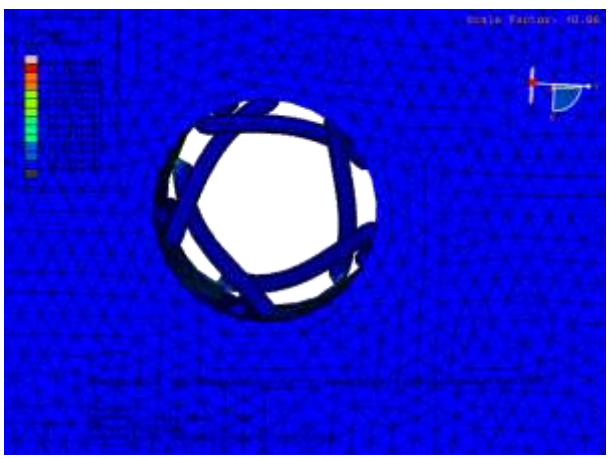


t=0.57

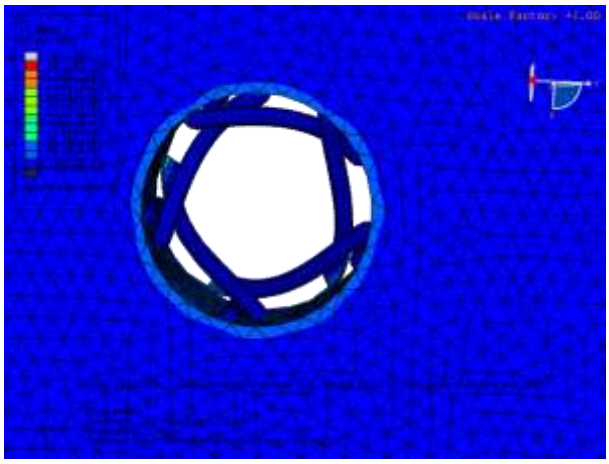


t=0.71

Figure 31, *contd.*



t=0.86



t=1

Figure 31: Gating transition of the membrane channel at different time points (t=0 through t=1 s).

Table 6: Results of In-plane Stress Analysis

Feature	**Original Diameter (A°)**	**New Diameter (A°)**	**% Change**	**Nodes**
Membrane Hole	**47.73**	**77.93**	**62.273**	**962:946**
Channel	**22.11**	**63.83**	**188.693**	**3178:10875**

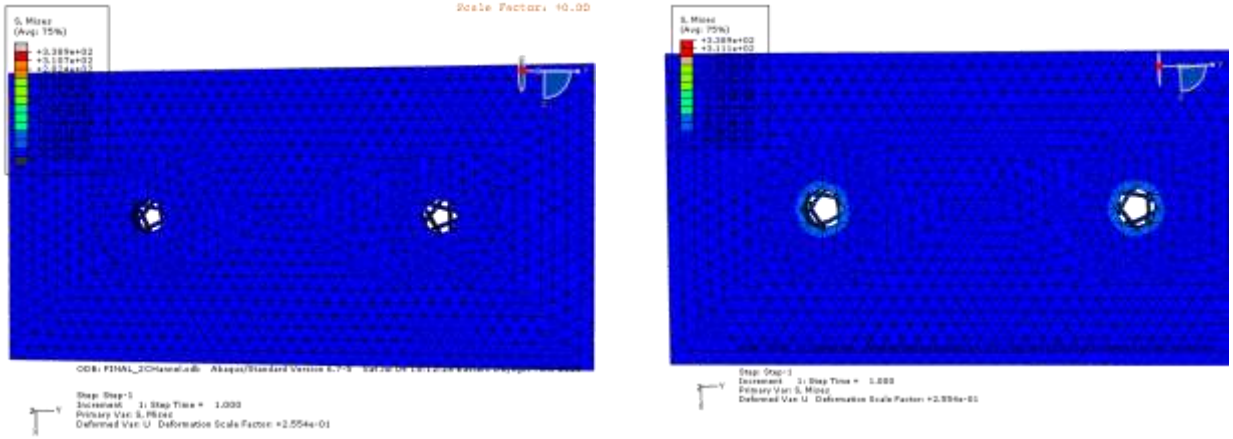
5.1.3.2 In-plane Stretch - Two-channel Model

The second step in the first stage of analysis involved applying the in-plane tension to a two-channel membrane-channel model. The same tension of 35 MPa that was applied to the single-channel model was applied here as well. The first two images in Figure 32 depict the initial state (prior to the application of load) and the final end state. The time period of the simulation was set to 1sec and 7 frames were established to check the transition of the results. The frames represent results at t = 0, 0.14, 0.29, 0.43, 0.57, 0.71, 0.86, 1 s. Table 7 following the frames presents the change in diameter of the hole and the channel. As was discussed earlier, the radius of the channel is the most important variable measured to study the gating mechanism of a channel; the change in diameter of the various structures is mentioned after the pictorial results. The nodes mentioned in the results are the nodes that are diametrically opposite each other.

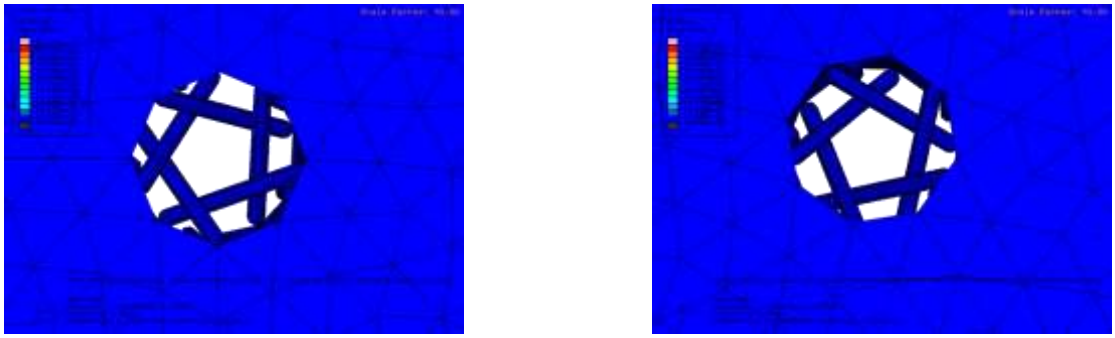
5.1.3.3 Out-of-plane Bending - +ve Z-direction

The next step in the first stage of the analysis was to apply the second type of loading on to the Membrane-Channel Model, both the single and the two-channel models. Bending was achieved by applying a bending force as calculated in the loads section previously. To check for the directional dependency of the model, the force was applied both in the positive and negative directions. The current section, as the name suggests, gives results for bending in the positive Z direction. Figure 35 represents the frame results at t = 0, 0.14, 0.29, 0.43, 0.57, 0.71, 0.86, 1 s. Table 8 following the frames presents the change in diameter of the hole and the channel. As was discussed earlier, the radius of the channel is the most important variable measured to study the gating mechanism of a channel; the change in diameter of the various structures is mentioned after the pictorial results. The nodes mentioned in the table are diametrically opposite to each other.

Initial State **End State**



t=0



t=0.14

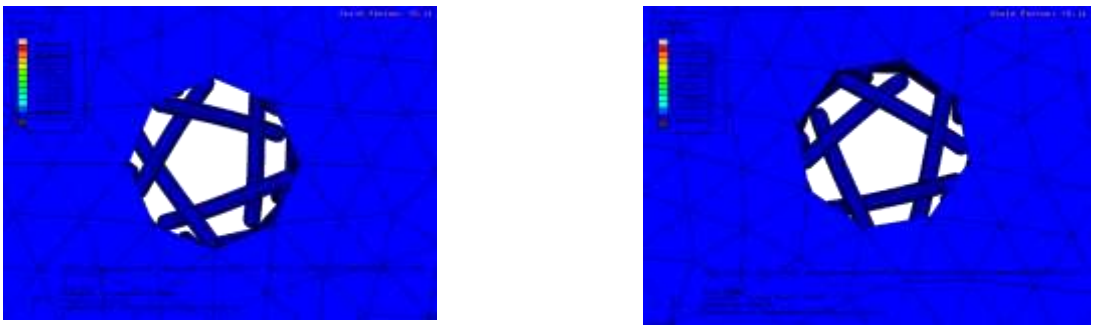
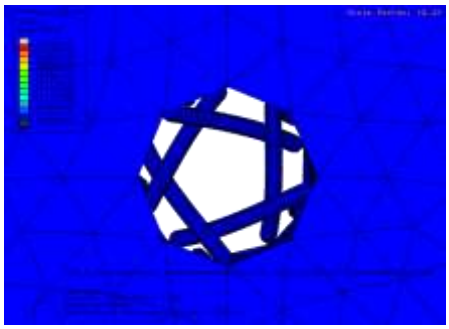
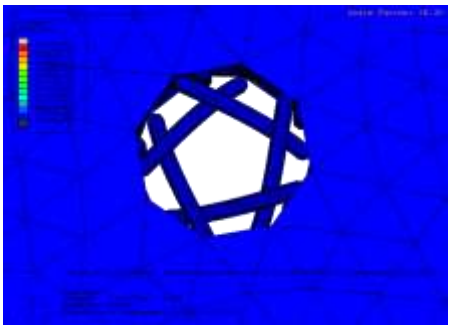


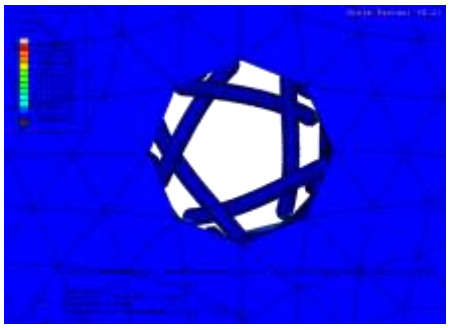
Figure 32, *contd.*

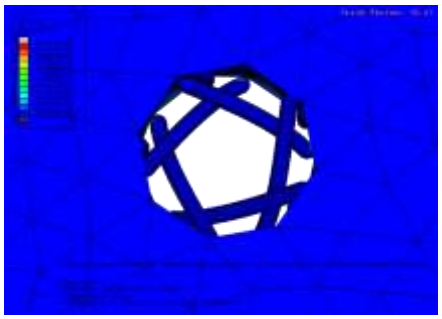
t=0.29



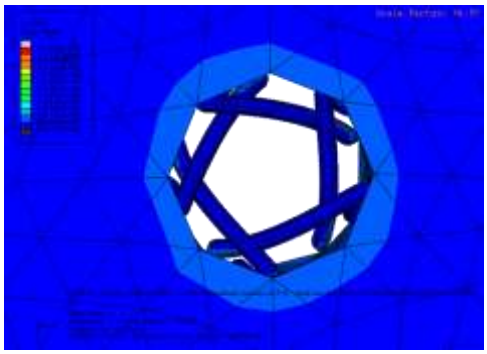


t=0.43





t=0.57



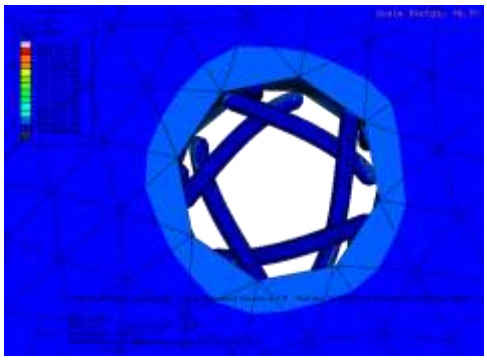
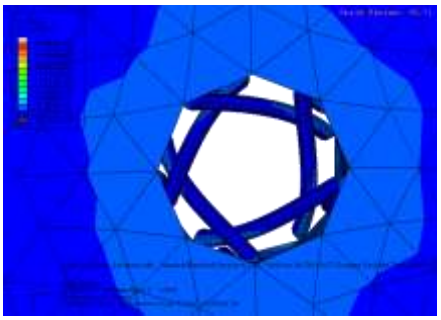
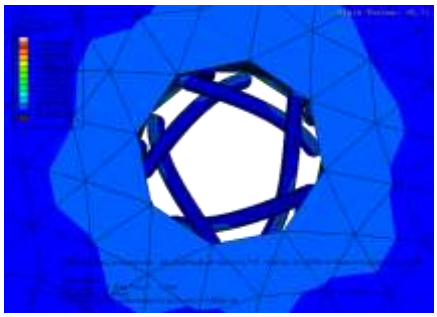


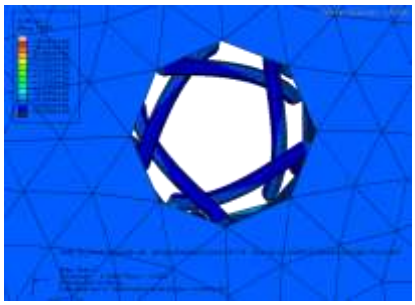
Figure 32, *contd.*

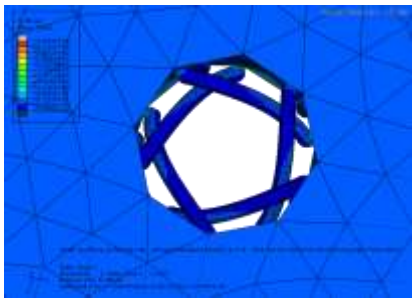
t=0.71



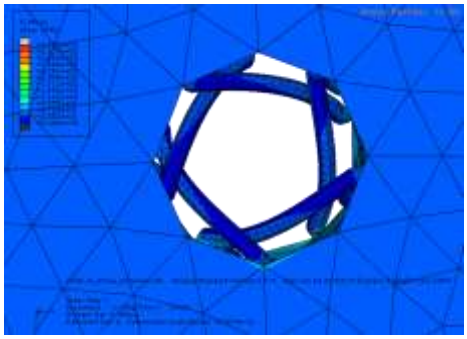


t=0.86





t=1



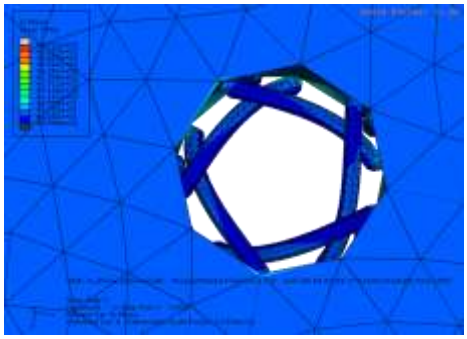
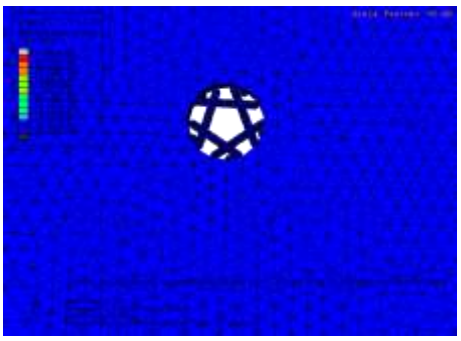


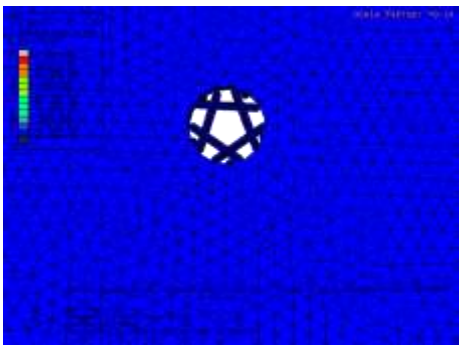
Figure 32: Gating transition of the two-channel model at different time points (t= 0 through 1 s).

Table 7: Results of the Analysis

Feature	Original Diameter (A°)	New Diameter (A°)	% Change	Nodes
Membrane Hole 1	**48**	**76.5**	**59.375**	**294:290**
Membrane Hole 2	**48**	**76.5**	**59.375**	**591:587**
Channel 1	**23.13**	**56.8**	**145.569**	**940:1442**
Channel 2	**22.04**	**57.54**	**149.740**	**1654:3522**

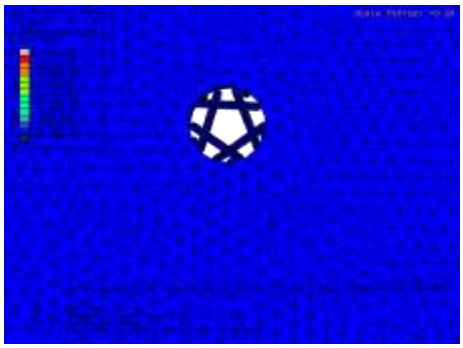


t=0

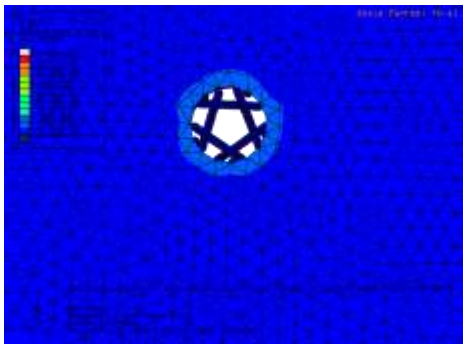


t=0.14

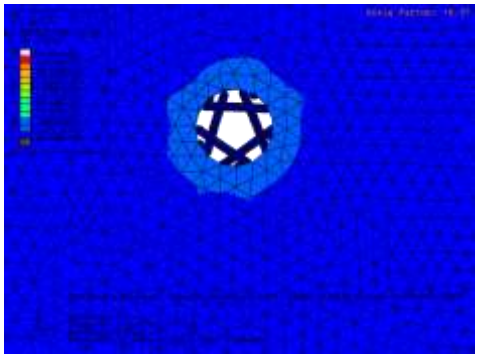
Figure 33



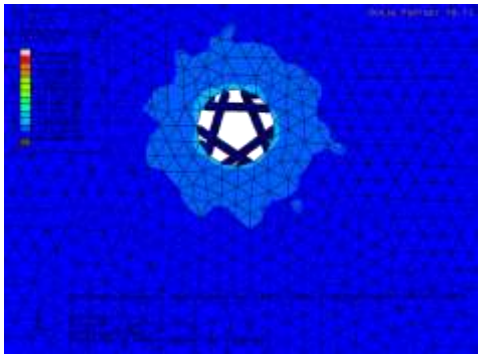
t=0.29



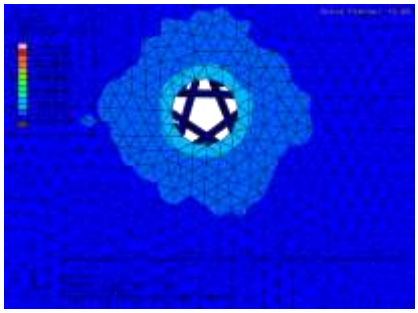
t=0.43



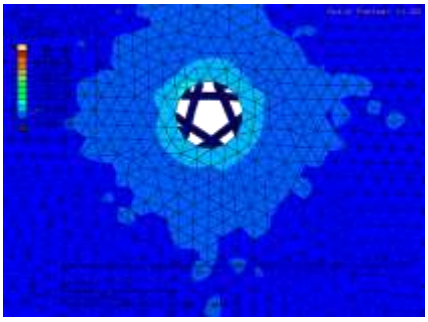
t=0.57



t=0.71



t=0.86



t=1

Figure 33: Gating transition at different time points (in sec) after application of out of plane bending in the + Z direction to the membrane channel model.

Table 8: Results of the Analysis

Feature	Original Diameter (A°)	New Diameter (A°)	% Change	Nodes
Membrane Hole	**47.73**	**44.19**	**-7.417**	**569:577**
	47.73	**44.23**	**-7.333**	**52:573**
Channel	**22.1**	**23.39**	**6.244**	**4337:3974**
	22.1	**23.07**	**4.389**	**1346:3969**

5.1.3.4 Out-of-plane Bending - -ve Z-direction

As has been mentioned in the previous section, this section applies the same bending force but in the negative Z direction. Figure 34 represents the frame results at t = 0, 0.14, 0.29, 0.43, 0.57, 0.71, 0.86, 1 s. Table 9 following the frames presents the change in diameter of the hole and the channel. As was discussed earlier, the radius of the channel is the most important variable measured to study the gating mechanism of a channel; the change in diameter of the various structures is mentioned after the pictorial results. The nodes mentioned in the table are diametrically opposite to each other.

5.1.3.5 Out-of-plane Bending - +ve Z-direction - Two-channel Model

As was done for the in-plane stretching analysis, the bending analysis was also performed on the two-channel model. Bending was achieved by applying a bending force as calculated in the loads section previously. To check for the directional dependency of the model as was done to the single channel model, the force was applied both in the positive and negative directions. The current section, as the name suggests, gives the results for bending in the positive Z direction. Figure 35 represents the frame results at t = 0, 0.14, 0.29, 0.43, 0.57, 0.71, 0.86, 1 s. Table 10 following the frames presents the change in diameter of the hole and the channel. As was discussed earlier, the radius of the channel is the most important variable measured to study the gating mechanism of a channel; the change in diameter of the various structures is mentioned after the pictorial results. The nodes mentioned in the table are diametrically opposite to each other.

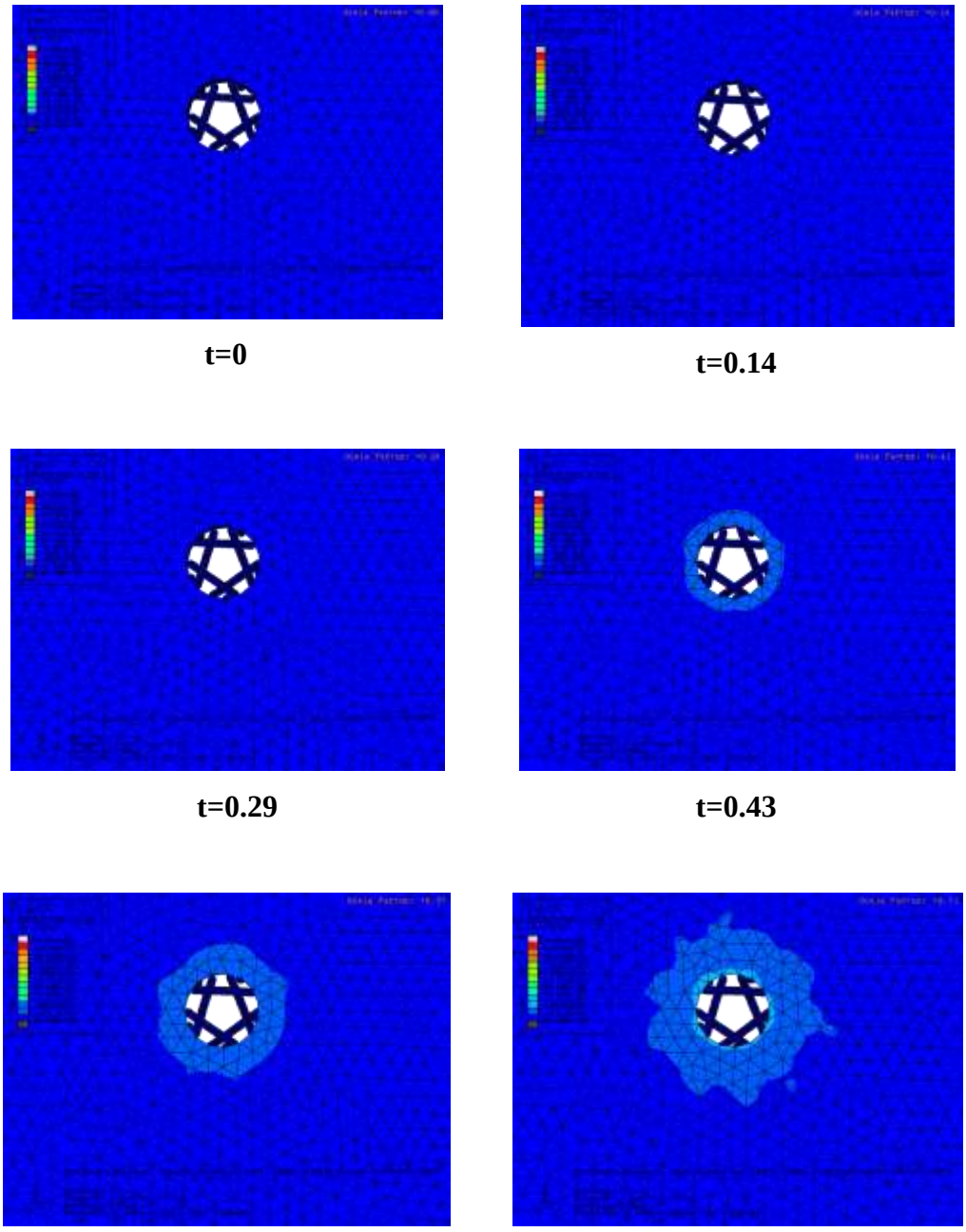
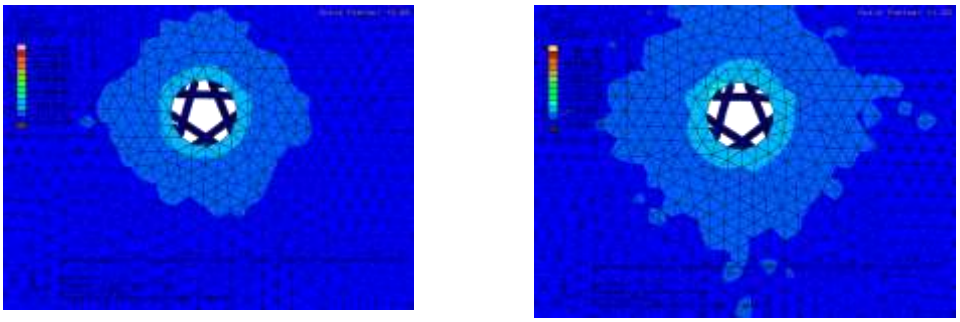


Figure 34



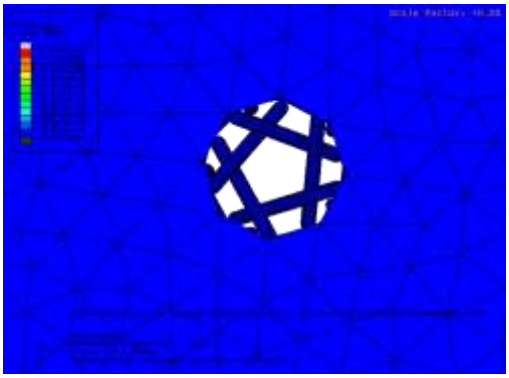
t=0.86 **t=1**

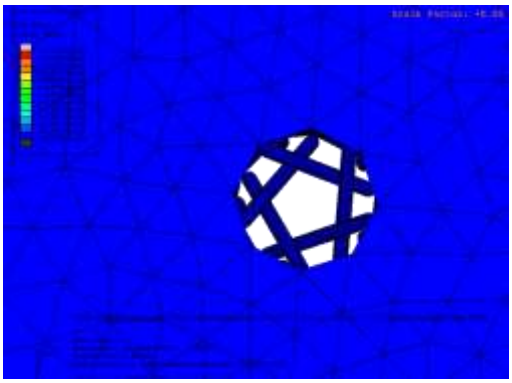
Figure 34: Gating transition at different time points (in sec) after application of out of plane bending in the -Z direction to the membrane channel model.

Table 9: Results of the Analysis

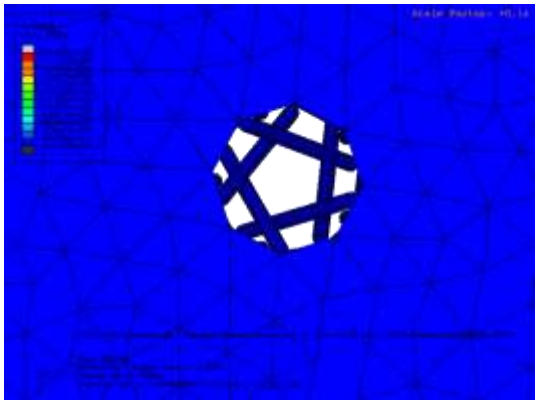
Feature	Original Diameter (A°)	New Diameter (A°)	% Change	Nodes
Membrane Hole	**47.73**	**51.27**	**7.417**	**569:577**
	47.73	**51.23**	**7.333**	**52:573**
Channel	**22.1**	**20.59**	**-6.833**	**4337:3974**
	22.1	**21.18**	**-4.163**	**1346:3969**

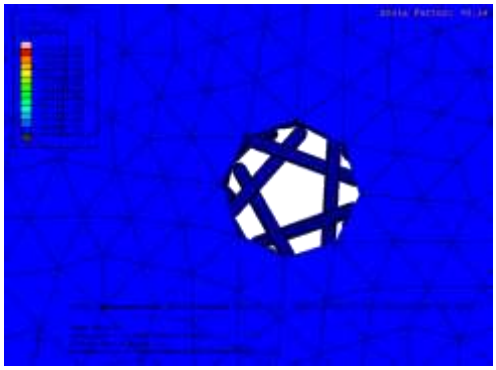
t=0



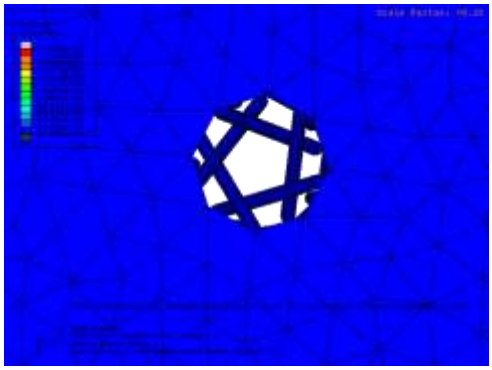


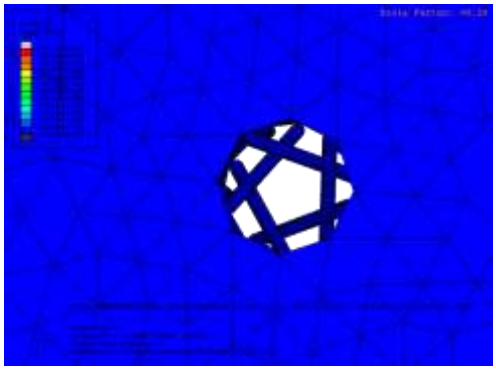
t=0.14





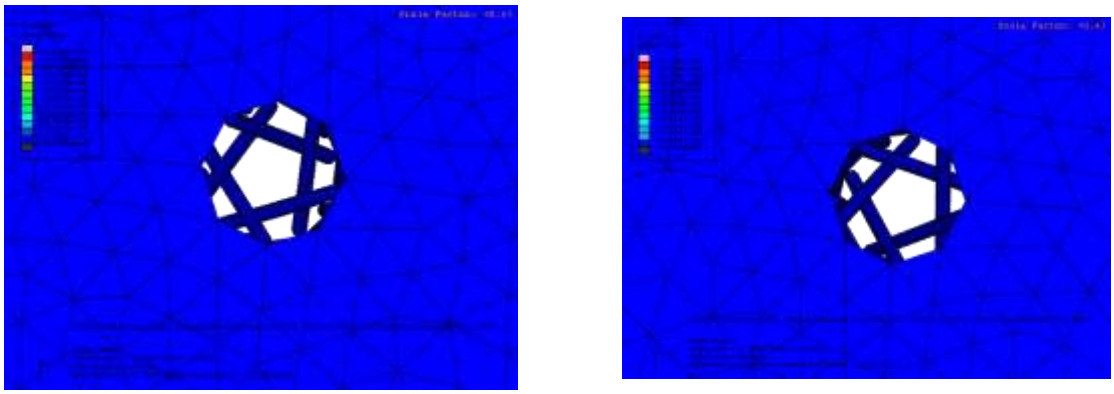
t=0.29



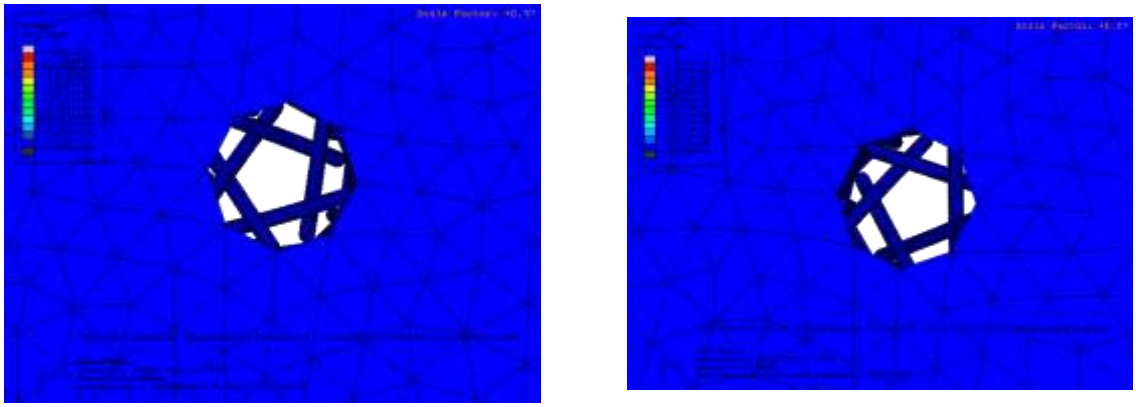


t=0.43

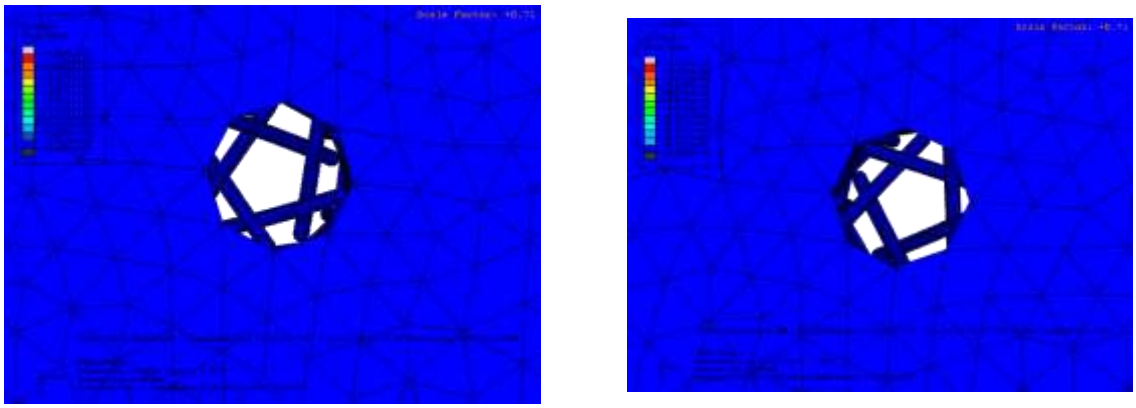
Figure 35



t=0.57



t=0.71



t=0.86

Figure 35, *contd.*

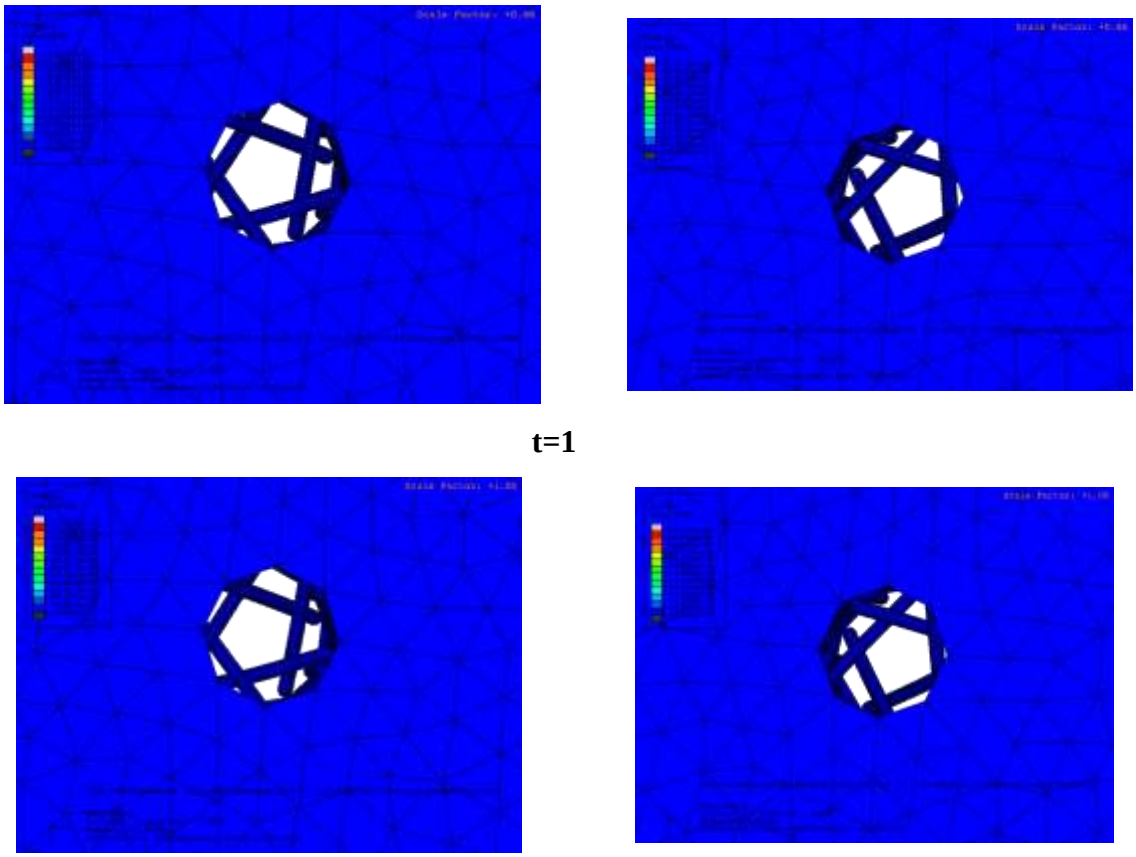


Figure 35: Gating transition at different time points (in sec) after application of out-of-plane bending in the +Z direction to the two channel model.

Table 10: Results of the Analysis

Feature	Original Diameter (A°)	New Diameter (A°)	% Change	Nodes
Membrane	**48**	**46.9**	**-2.292**	**294:290**
Hole	**48**	**46.9**	**-2.292**	**591:587**
Channel	**22.1**	**24.02**	**8.688**	**940:1442**
	22.1	**24.04**	**8.778**	**1654:3522**

5.1.3.6 Out-of-plane Bending - -ve Z-direction - Two-channel Model

As was mentioned in the previous section, in the current section, the bending force was applied in the –ve Z-direction. Figure 36 represents the frame results at t = 0, 0.14, 0.29, 0.43, 0.57, 0.71, 0.86, 1 s. Table 11 following the frames presents the change in diameter of the hole and the channel. As was discussed earlier, the radius of the channel is the most important variable measured to study the gating mechanism of a channel; the change in diameter of the various structures is mentioned after the pictorial results. The nodes mentioned in the table are diametrically opposite to each other.

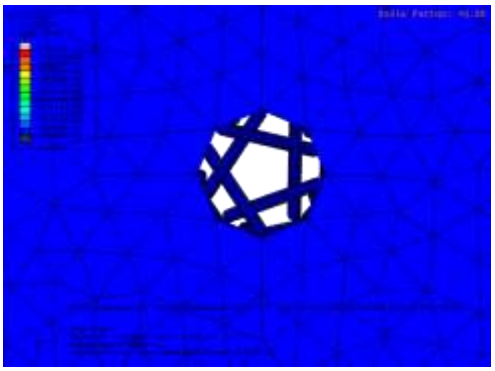
5.2 The Heart Model

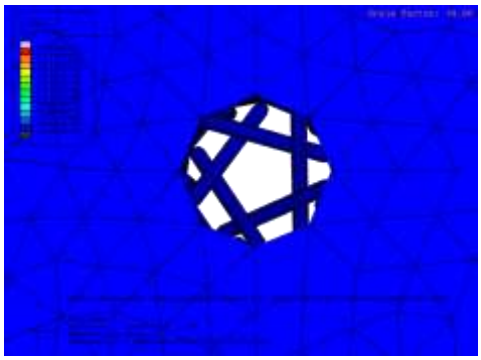
One major aim of the current analysis is to better understand the mechanism of c*ommotio cordis,* a state that leads to sudden cardiac failure especially in athletes due to a low intensity blow to the chest. Timing is crucial for this phenomenon to occur. To better understand the stress profile of the heart due to a blow to the chest, an accurate model of a human heart was subjected to an external load and the stress was noted down. These stress values were then applied to the single-channel membrane to check if that tension is capable of causing the channel to open.

5.2.1 Boundary Conditions

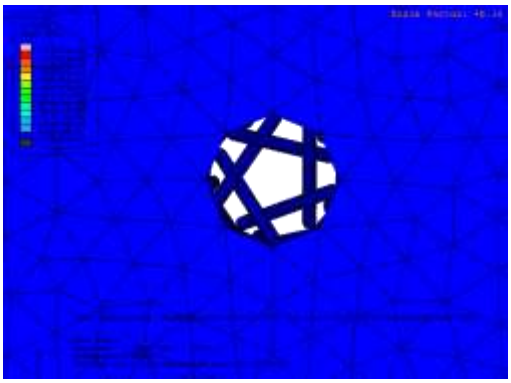
As the heart does not move away from its location on impact, but merely absorbs and deforms at the same place, so the area near the aorta and the area around the base of the heart were pinned, thus the model as a whole would not move but the region that was under observation, i.e. all the degrees of freedom for the atria and ventricles were intact. Figure 37 illustrates the boundary condition applied on the model.

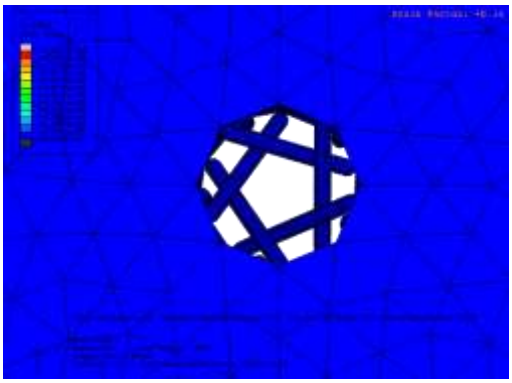
t=0



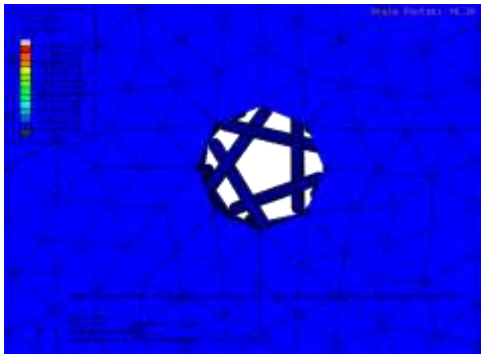


t=0.14





t=0.29



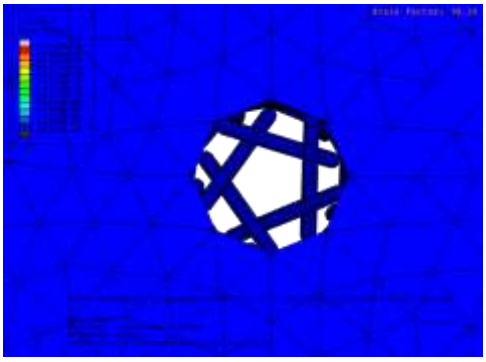
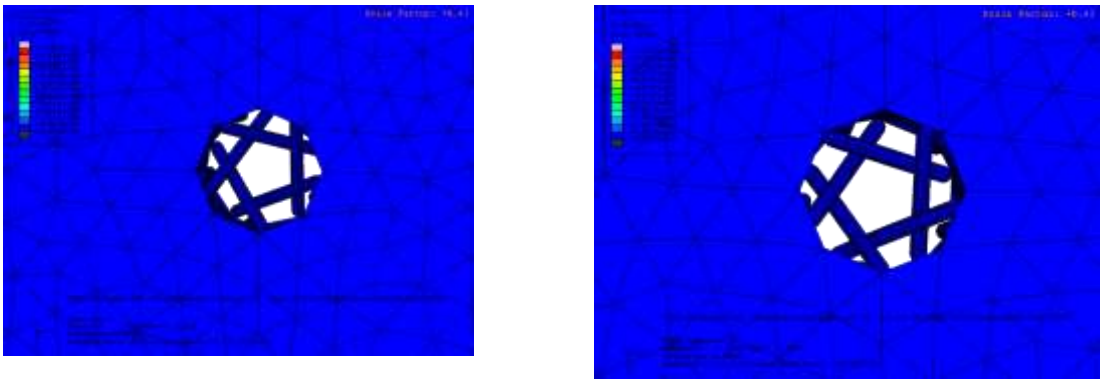
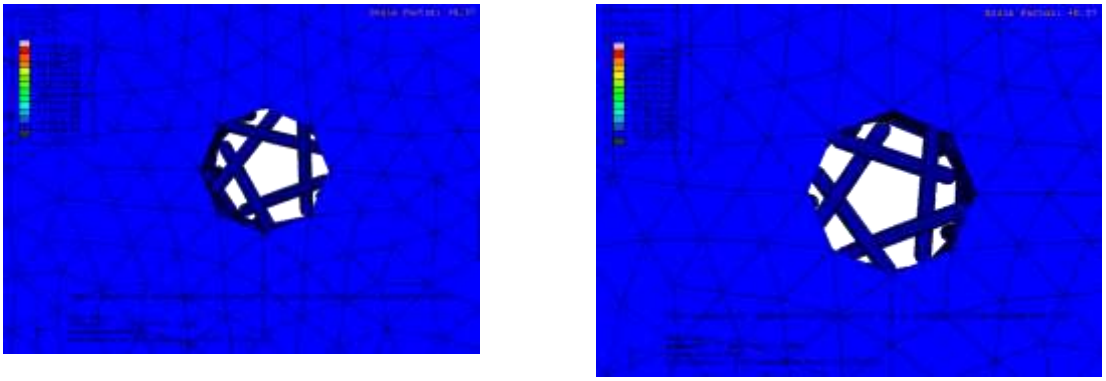


Figure 36

t=0.43



t=0.57



t=0.71

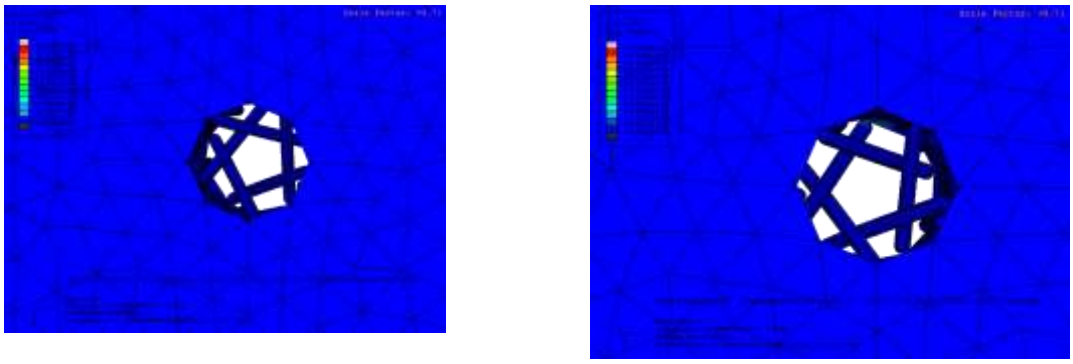
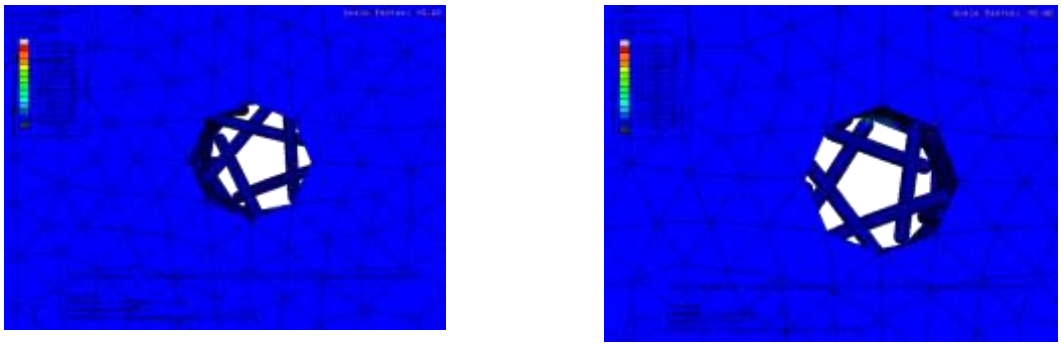


Figure 36, *contd.*

t=0.86



t=1

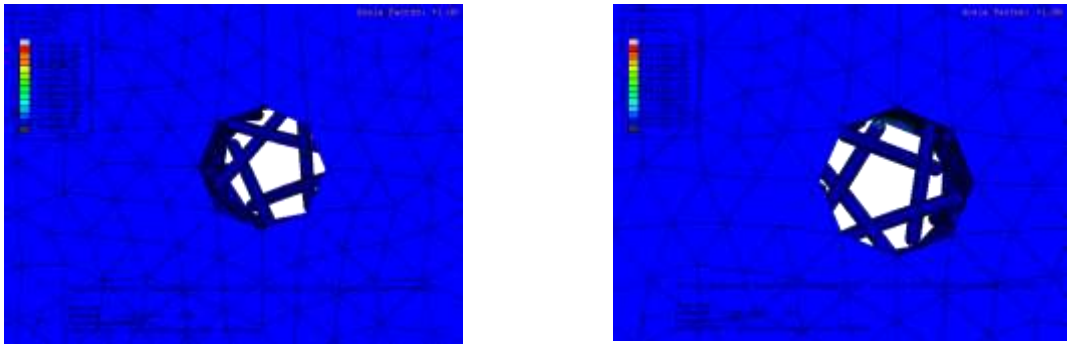
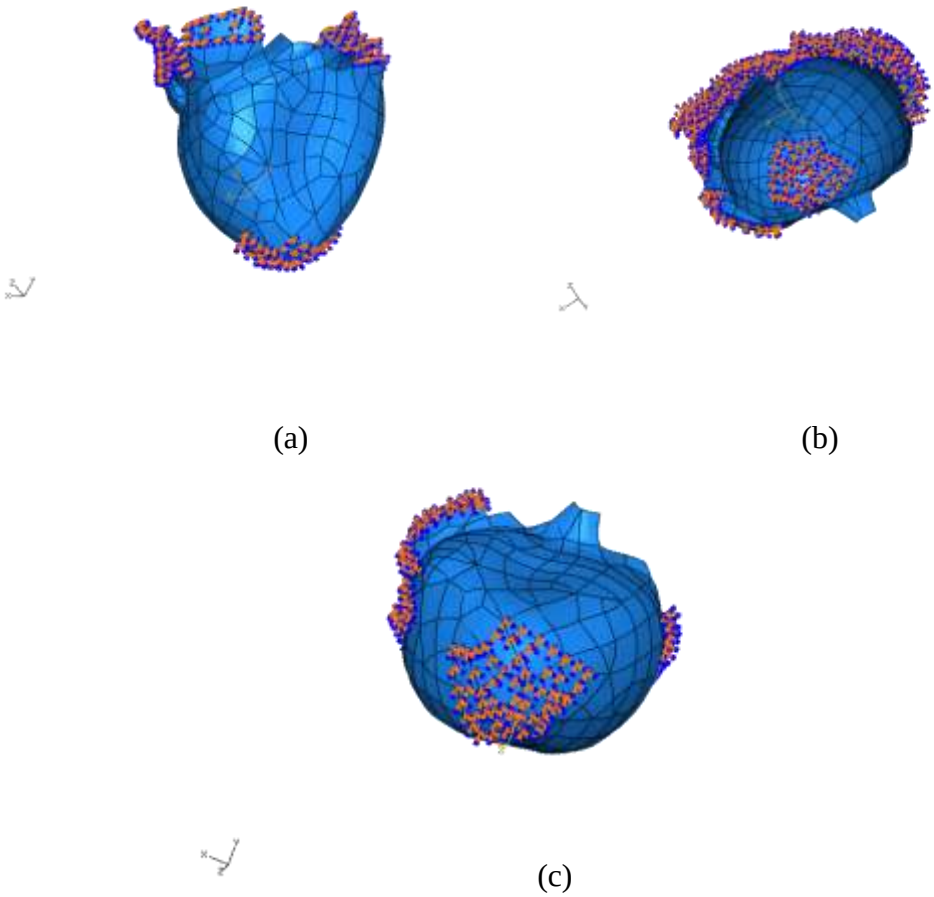


Figure 36: Gating transition at different time points (in sec) after application of out-of-plane bending in the -Z-direction to the two-channel model.

Table 11: Results of the Analysis

Feature	Original Diameter (A°)	New Diameter (A°)	% Change	Nodes
Membrane	**48**	**51.5**	**7.292**	**294:290**
Hole	**48**	**51.5**	**7.292**	**591:587**
Channel	**22.1**	**20.59**	**-6.833**	**940:1442**
	22.1	**21.18**	**-4.163**	**1654:3522**



(a) (b)

(c)

Figure 37: (a), (b) and (c) represent different three-dimensional views of boundary conditions applied to the heart model.

5.2.2 Applied Loads and Results

The first step in this analysis involved emulating the effect of a human hand blow to the chest. To achieve this, a hypothetical mass of 1 Kg was assumed to travel at 40 mph and the time-period was set to 1 sec. These values were used to calculate the force of impact onto the chest. This force was then applied to the Membrane-Channel model to verify the change in channel radius. The calculations used to attain this result are mentioned below. All the values and assumptions taken here to calculate the force of impact are hypothetical. The main intention is to calculate force value that might be close to a real-life scenario and then applying that force to the membrane to check the change in radius. One major assumption here is that the force of impact is directly fed to the channel, this however is not true as there are other structures like the rib-cage, muscle, etc. that absorb a significant amount of the blow. Using the basic laws of physics the force of impact can be calculated as 17.88 N. Next, it is assumed that the object has a cross-sectional area of 1mm (indicates a sharp object), and the force per unit area is thus computed to be 17.88 MPa which was then transferred to the heart model. The heart model was subjected to 4 different points of impact as seen in Figure 38. This was performed to create a stress profile of the heart and also to choose the maximum available load to be transferred to the membrane-channel model.

$$\text{Mass} = 1 \text{ Kg}$$

$$\text{Assume, } V = 40 \text{ mph} = 64.37 \text{ Kmph} = 17.88 \text{ m/s}$$

$$\text{Assume, } t = 1 \text{ s}$$

$$V = at$$

$$17.88 = (a)\ (1)$$

$$a = 17.88 \text{ m/s}^2$$

$$F = m*a$$

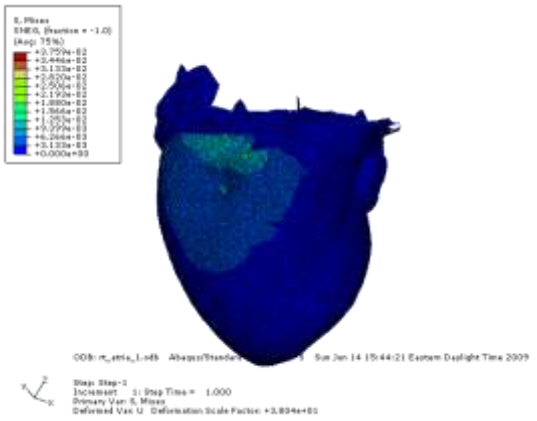
$$= 1*17.88$$

$$= 17.88 \text{ N}$$

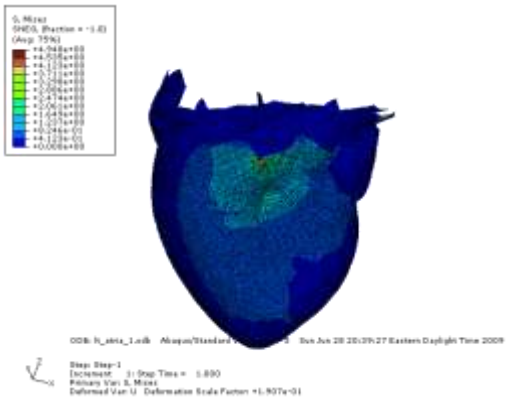
$$P = F/A$$

$$= 17.88/(10^{-3})^2$$

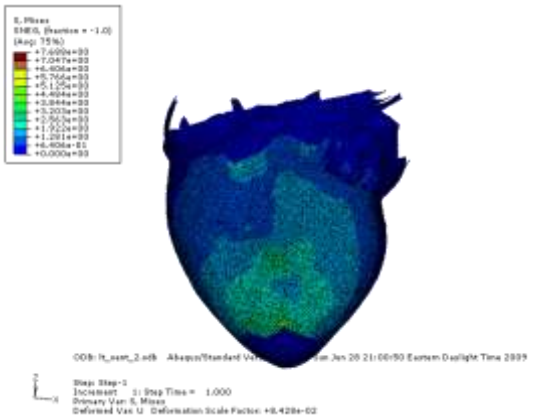
$$= 17.88 \text{ MPa}$$



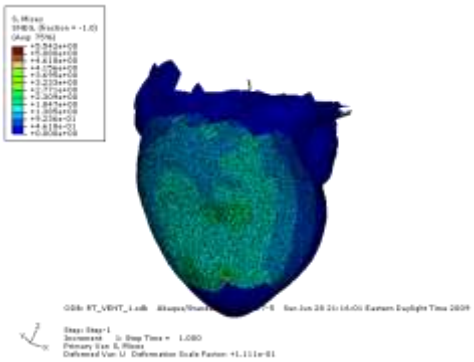
Impact on Rt Atria (max: 13.99MPa)



Impact on Lt Atria (max: 4.9MPa)



Impact on Rt Ventricle (max: 5.5MPa)



Impact on Lt Ventricle (max: 7.68MPa)

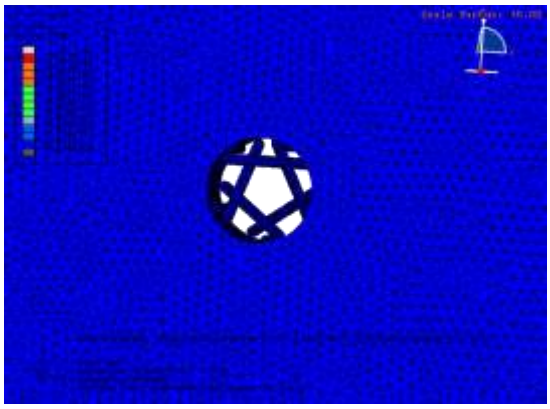
Figure 38: Impact on the chest at various points.

The next step in the analysis involved applying the maximum stress obtained from among the 4 different tests on the heart model. The maximum stress obtained was observed in the Rt Atria test with a magnitude of 13.99 MPa. This was then applied as in-plane stress on the edges of the Membrane-Channel model. Figure 39 represents the time intervals at t= 0, 0.14, 0.29, 0.43, 0.57, 0.71, 0.86, 1 s. Table 12 accompanying Figure 39 depicts the change in diameter at the nodes it has been measured.

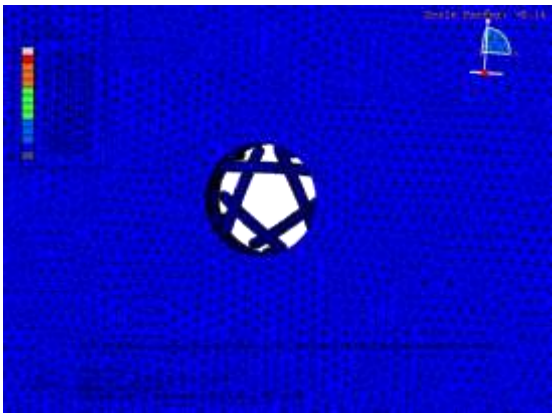
5.3 Discussion of Results

This section deals with the significance of the results obtained. The aim of this study was to build a simple 3D CAD model of a mechanosensitive channel and based on the results obtained, it can be said with confidence that although the results might be slightly off with experimental data, , the mechanism of the channel's opening closely matches that of the models provided by earlier researchers (Sukharev., (2004)). The membrane-channel model shows a decrease in thickness of about 26% after the application of in-plane stretch, this is in accordance with Perozo et al., (2002), who measured that the thickness of MscL changes by 20% after the application of a load. One other aspect of the results that increases the value of this model is the close match between the obtained between the single and the two-channel model. Both models displayed similar characteristics on the application of load; however, the two-channel model had a slightly lesser change in the diameter which could be explained by the fact that the same tension was applied to two different shapes.

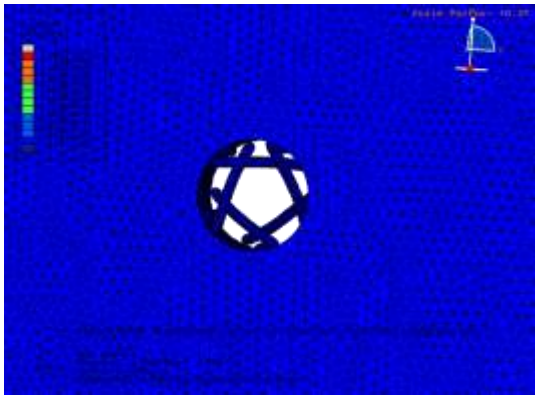
The other aspect of the analysis that involved the application of bending force on the model successfully elucidated the fact that tension within the lipid membrane is the primary driving force for the gating mechanism. All the simulations, both in the positive and the negative directions have not yielded any appreciable change in channel's radius. This result was also observed in the two-channel model, where the change in radius is in accordance with the single channel. It can also be observed that for both the models, the tilting of TM1 helix is more



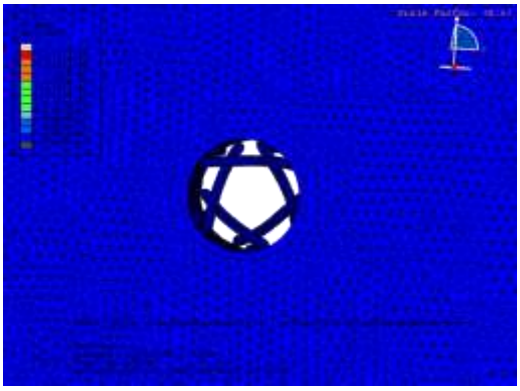
t=0



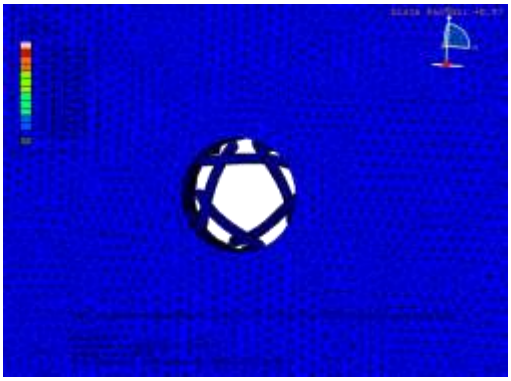
t=0.14



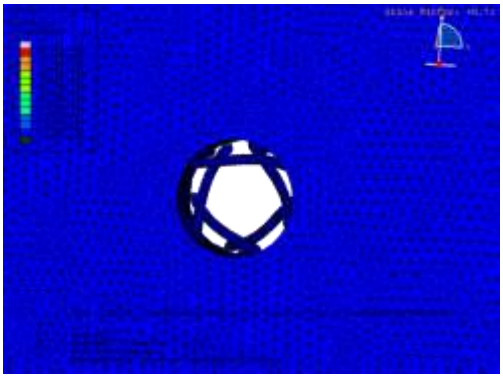
t=0.29



t=0.43

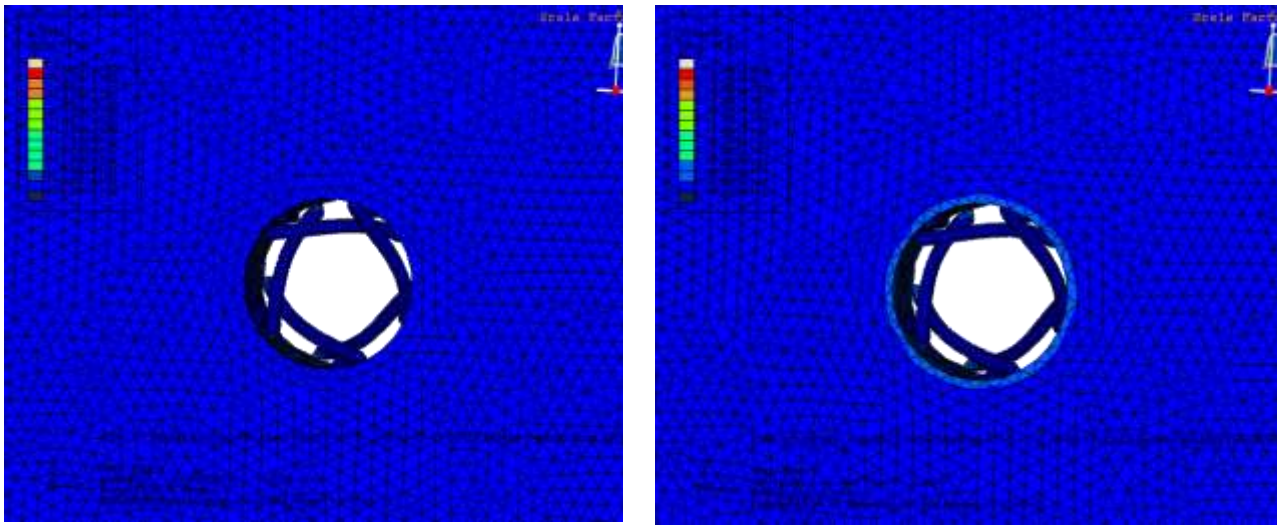


t=0.57



t=0.71

Figure 39



t=0.86 **t=1**

Figure 39: Applying the results of the Heart analysis to the Membrane-Channel model. Figure presents frames at t= 0 through 1 s.

Table 12: Results of the Analysis

Feature	Original Diameter (A°)	New Diameter (A°)	% Change	Nodes
Membrane Hole	**47.73**	**60.54**	**26.838**	**962:946**
Channel	**22.11**	**38.47**	**73.994**	**3178:10875**

significant than TM2, as TM2 acts more like a support structure in helping the TM1 bundle open. Better design that conforms to the real structure of the channel will help better understand the relation between the helices.

The second part of the analysis deals with the development of a stress profile of the heart. The application of this stress to the membrane-channel model shows the immense advantage and flexibility of using finite element modeling. The results from this mode show that, although the channel opens to a lesser extent, there is still a possibility that exchange of ions could be initiated that would ultimately lead to a change in the state of the whole cell, thereby causing depolarization to occur abruptly, ultimately leading to arrhythmias.

CHAPTER VI Future Directions

The results obtained with the simplistic model are remarkable and glorifies the use of the Finite Element Modeling Technique. However, this simulation does not take into consideration molecular level interactions and thus has its own limitations. This analysis was an exercise to display the effectiveness of the Finite Element modeling technique in solving a biological phenomenon. As from the very beginning, it has been stated that the analysis was performed on a highly simplified model of the channel that basically transformed a biological problem into a mechanical problem. So, there are many aspects, if improved on, will help in the application of this technique to study and postulate theories to explain the numerous anomalies that are yet to be explained with regard to the mechanical response of the human heart.

The first advancement that would incredibly improve the quality of the results would be to increase the complexity of the membrane. As has been mentioned earlier, the membrane is the single most important component in the gating mechanism and having a better representation will help converge on a more realistic result. The use of multiple layers with different properties sandwiched together can be a good representation of the lipid membrane. Also incorporation of interaction properties between the layers would also add to the quality of results.

Another field of improvement would be to model the helices with their potentials into consideration i.e. their hydrostatic and hydrophobic ends as previous studies have revealed that these potential differences also have an important role to play in the gating mechanism of the channel. As the trigger mechanism of these channels are still not well understood, applying different types of loads, for example, an oscillating mechanical load, osmotic pressure, etc. can be applied in a Finite Element framework.

The current study applies a static approach in solving the problem. However, the future analysis can very well include other variables like temperature, pressure, regional polarity, etc.

List of References

1. **Anishkin, A., V. Gendel, N. A. Sharifi, C. S. Chiang, L. Shirinian, H. R. Guy, and S. Sukharev.** 2003. On the conformation of the COOH-terminal domain of the large mechanosensitive channel MscL. J Gen Physiol **121:**227-244.
2. **Ayoub, I. M., J. Kolarova, Z. Yi, A. Trevedi, H. Deshmukh, D. L. Lubell, M. R. Franz, F. A. Maldonado, and R. J. Gazmuri.** 2003. Sodium-hydrogen exchange inhibition during ventricular fibrillation: Beneficial effects on ischemic contracture, action potential duration, reperfusion arrhythmias, myocardial function, and resuscitability. Circulation **107:**1804-1809.
3. **Bainbridge, F. A.** 1915. The influence of venous filling upon the rate of the heart. J Physiol **50:**65-84.
4. **Bathe, M.** 2008. A finite element framework for computation of protein normal modes and mechanical response. Proteins **70:**1595-1609.
5. **Befeler, B.** 1978. Mechanical stimulation of the heart: its therapeutic value in tachyarrhythmias. Chest **73:**832-838.
6. **Bett, G. C., and F. Sachs.** 2000. Whole-cell mechanosensitive currents in rat ventricular myocytes activated by direct stimulation. J Membr Biol **173:**255-263.
7. **Bilston, L. E., and K. Mylvaganam.** 2002. Molecular simulations of the large conductance mechanosensitive (MscL) channel under mechanical loading. FEBS Lett **512:**185-190.
8. **Bode, F., F. Sachs, and M. R. Franz.** 2001. Tarantula peptide inhibits atrial fibrillation. Nature **409:**35-36.
9. **Chang, G., R. H. Spencer, A. T. Lee, M. T. Barclay, and D. C. Rees.** 1998. Structure of the MscL homolog from Mycobacterium tuberculosis: a gated mechanosensitive ion channel. Science **282:**2220-2226.
10. **Chen, X., Q. Cui, Y. Tang, J. Yoo, and A. Yethiraj.** 2008. Gating mechanisms of mechanosensitive channels of large conductance, I: a continuum mechanics-based hierarchical framework. Biophys J **95:**563-580.
11. **Chen, X. Z., P. M. Vassilev, N. Basora, J. B. Peng, H. Nomura, Y. Segal, E. M. Brown, S. T. Reeders, M. A. Hediger, and J. Zhou.** 1999. Polycystin-L is a calcium-regulated cation channel permeable to calcium ions. Nature **401:**383-386.

12. **Choe, S., and S. X. Sun.** 2005. The elasticity of alpha-helices. J Chem Phys **122:**244912.
13. **Cooper, P. J., A. Epstein, I. A. Macleod, S. T. Schaaf, J. Sheldon, C. Boulin, and P. Kohl.** 2006. Soft tissue impact characterisation kit (STICK) for ex situ investigation of heart rhythm responses to acute mechanical stimulation. Prog Biophys Mol Biol **90:**444-468.
14. **Debret, G., H. Valadie, A. M. Stadler, and C. Etchebest.** 2008. New insights of membrane environment effects on MscL channel mechanics from theoretical approaches. Proteins **71:**1183-1196.
15. **Elmore, D. E., and D. A. Dougherty.** 2003. Investigating lipid composition effects on the mechanosensitive channel of large conductance (MscL) using molecular dynamics simulations. Biophys J **85:**1512-1524.
16. **Franco, A., Jr., and J. B. Lansman.** 1990. Calcium entry through stretch-inactivated ion channels in mdx myotubes. Nature **344:**670-673.
17. **Franz, M. R., R. Cima, D. Wang, D. Profitt, and R. Kurz.** 1992. Electrophysiological effects of myocardial stretch and mechanical determinants of stretch-activated arrhythmias. Circulation **86:**968-978.
18. **Garny, A., and P. Kohl.** 2004. Mechanical induction of arrhythmias during ventricular repolarization: modeling cellular mechanisms and their interaction in two dimensions. Ann N Y Acad Sci **1015:**133-143.
19. **Garny, A., D. Noble, and P. Kohl.** 2005. Dimensionality in cardiac modelling. Prog Biophys Mol Biol **87:**47-66.
20. **Gullingsrud, J., D. Kosztin, and K. Schulten.** 2001. Structural determinants of MscL gating studied by molecular dynamics simulations. Biophys J **80:**2074-2081.
21. **Gullingsrud, J., and K. Schulten.** 2003. Gating of MscL studied by steered molecular dynamics. Biophys J **85:**2087-2099.
22. **Hansen, D. E., M. Borganelli, G. P. Stacy, Jr., and L. K. Taylor.** 1991. Dose-dependent inhibition of stretch-induced arrhythmias by gadolinium in isolated canine ventricles. Evidence for a unique mode of antiarrhythmic action. Circ Res **69:**820-831.

23. **Hansen, D. E., C. S. Craig, and L. M. Hondeghem.** 1990. Stretch-induced arrhythmias in the isolated canine ventricle. Evidence for the importance of mechanoelectrical feedback. Circulation **81:**1094-1105.

24. **Healy, S. N., and A. D. McCulloch.** 2005. An ionic model of stretch-activated and stretch-modulated currents in rabbit ventricular myocytes. Europace **7 Suppl 2:**128-134.

25. **Ingber, D. E.** 2006. Cellular mechanotransduction: putting all the pieces together again. FASEB J **20:**811-827.

26. **Kernan, M. J.** 2007. Mechanotransduction and auditory transduction in Drosophila. Pflugers Arch **454:**703-720.

27. **Kohl, P., C. Bollensdorff, and A. Garny.** 2006. Effects of mechanosensitive ion channels on ventricular electrophysiology: experimental and theoretical models. Exp Physiol **91:**307-321.

28. **Kohl, P., P. Hunter, and D. Noble.** 1999. Stretch-induced changes in heart rate and rhythm: clinical observations, experiments and mathematical models. Prog Biophys Mol Biol **71:**91-138.

29. **Kohl, P., A. D. Nesbitt, P. J. Cooper, and M. Lei.** 2001. Sudden cardiac death by Commotio cordis: role of mechano-electric feedback. Cardiovasc Res **50:**280-289.

30. **Kohler, R., A. Distler, and J. Hoyer.** 1999. Increased mechanosensitive currents in aortic endothelial cells from genetically hypertensive rats. J Hypertens **17:**365-371.

31. **Kong, Y., Y. Shen, T. E. Warth, and J. Ma.** 2002. Conformational pathways in the gating of Escherichia coli mechanosensitive channel. Proc Natl Acad Sci U S A **99:**5999-6004.

32. **Le Guennec, J. Y., N. Peineau, J. A. Argibay, K. G. Mongo, and D. Garnier.** 1990. A new method of attachment of isolated mammalian ventricular myocytes for tension recording: length dependence of passive and active tension. J Mol Cell Cardiol **22:**1083-1093.

33. **Levina, N., S. Totemeyer, N. R. Stokes, P. Louis, M. A. Jones, and I. R. Booth.** 1999. Protection of Escherichia coli cells against extreme turgor by activation of MscS and MscL mechanosensitive channels: identification of genes required for MscS activity. EMBO J **18:**1730-1737.

34. **Li, W., P. Kohl, and N. Trayanova.** 2004. Induction of ventricular arrhythmias following mechanical impact: a simulation study in 3D. J Mol Histol **35:**679-686.

35. **Link, M. S., P. J. Wang, N. G. Pandian, S. Bharati, J. E. Udelson, M. Y. Lee, M. A. Vecchiotti, B. A. VanderBrink, G. Mirra, B. J. Maron, and N. A. Estes, 3rd.** 1998. An experimental model of sudden death due to low-energy chest-wall impact (commotio cordis). N Engl J Med **338:**1805-1811.

36. **Link, M. S., P. J. Wang, B. A. VanderBrink, E. Avelar, N. G. Pandian, B. J. Maron, and N. A. Estes, 3rd.** 1999. Selective activation of the K(+)(ATP) channel is a mechanism by which sudden death is produced by low-energy chest-wall impact (Commotio cordis). Circulation **100:**413-418.

37. **Madias, C., B. J. Maron, S. Supron, N. A. Estes, 3rd, and M. S. Link.** 2008. Cell membrane stretch and chest blow-induced ventricular fibrillation: commotio cordis. J Cardiovasc Electrophysiol **19:**1304-1309.

38. **Markhasin, V. S., O. Solovyova, L. B. Katsnelson, Y. Protsenko, P. Kohl, and D. Noble.** 2003. Mechano-electric interactions in heterogeneous myocardium: development of fundamental experimental and theoretical models. Prog Biophys Mol Biol **82:**207-220.

39. **Maroto, R., A. Raso, T. G. Wood, A. Kurosky, B. Martinac, and O. P. Hamill.** 2005. TRPC1 forms the stretch-activated cation channel in vertebrate cells. Nat Cell Biol **7:**179-185.

40. **Martinac, B.** 2004. Mechanosensitive ion channels: molecules of mechanotransduction. J Cell Sci **117:**2449-2460.

41. **Matthews, B. D., D. R. Overby, R. Mannix, and D. E. Ingber.** 2006. Cellular adaptation to mechanical stress: role of integrins, Rho, cytoskeletal tension and mechanosensitive ion channels. J Cell Sci **119:**508-518.

42. **Meyer, G. R., J. Gullingsrud, K. Schulten, and B. Martinac.** 2006. Molecular dynamics study of MscL interactions with a curved lipid bilayer. Biophys J **91:**1630-1637.

43. **Ninio, D. M., K. J. Murphy, P. R. Howe, and D. A. Saint.** 2005. Dietary fish oil protects against stretch-induced vulnerability to atrial fibrillation in a rabbit model. J Cardiovasc Electrophysiol **16:**1189-1194.

44. **Pascarel, C., K. Hongo, O. Cazorla, E. White, and J. Y. Le Guennec.** 1998. Different effects of gadolinium on I(KR), I(KS) and I(K1) in guinea-pig isolated ventricular myocytes. Br J Pharmacol **124:**356-360.

45. **Perozo, E., D. M. Cortes, P. Sompornpisut, A. Kloda, and B. Martinac.** 2002. Open channel structure of MscL and the gating mechanism of mechanosensitive channels. Nature **418:**942-948.

46. **Rickheit, G., H. Maier, N. Strenzke, C. E. Andreescu, C. I. De Zeeuw, A. Muenscher, A. A. Zdebik, and T. J. Jentsch.** 2008. Endocochlear potential depends on Cl- channels: mechanism underlying deafness in Bartter syndrome IV. EMBO J **27:**2907-2917.

47. **Rodriguez, B., and N. Trayanova.** 2003. Upper limit of vulnerability in a defibrillation model of the rabbit ventricles. J Electrocardiol **36 Suppl:**51-56.

48. **Stokes, N. R., H. D. Murray, C. Subramaniam, R. L. Gourse, P. Louis, W. Bartlett, S. Miller, and I. R. Booth.** 2003. A role for mechanosensitive channels in survival of stationary phase: regulation of channel expression by RpoS. Proc Natl Acad Sci U S A **100:**15959-15964.

49. **Sukharev, S., and A. Anishkin.** 2004. Mechanosensitive channels: what can we learn from 'simple' model systems? Trends Neurosci **27:**345-351.

50. **Sukharev, S., M. Betanzos, C. S. Chiang, and H. R. Guy.** 2001. The gating mechanism of the large mechanosensitive channel MscL. Nature **409:**720-724.

51. **Tang, Y., G. Cao, X. Chen, J. Yoo, A. Yethiraj, and Q. Cui.** 2006. A finite element framework for studying the mechanical response of macromolecules: application to the gating of the mechanosensitive channel MscL. Biophys J **91:**1248-1263.

52. **Tang, Y., J. Yoo, A. Yethiraj, Q. Cui, and X. Chen.** 2008. Gating mechanisms of mechanosensitive channels of large conductance, II: systematic study of conformational transitions. Biophys J **95:**581-596.

53. **Tang, Y., J. Yoo, A. Yethiraj, Q. Cui, and X. Chen.** 2008. Mechanosensitive channels: insights from continuum-based simulations. Cell Biochem Biophys **52:**1-18.

54. **Teichmann, M., I. Darcy, A. C. Bachoud-Levi, and E. Dupoux.** 2009. The role of the striatum in phonological processing. Evidence from early stages of Huntington's disease. Cortex **45:**839-849.

55. **Van Wagoner, D. R., and M. Lamorgese.** 1994. Ischemia potentiates the mechanosensitive modulation of atrial ATP-sensitive potassium channels. Ann N Y Acad Sci **723:**392-395.

56. **Wang, H., and G. Oster.** 1998. Energy transduction in the F1 motor of ATP synthase. Nature **396:**279-282.

57. **Wiggins, P., and R. Phillips.** 2004. Analytic models for mechanotransduction: gating a mechanosensitive channel. Proc Natl Acad Sci U S A **101:**4071-4076.

58. **Zumdieck, A., M. Cosentino Lagomarsino, C. Tanase, K. Kruse, B. Mulder, M. Dogterom, and F. Julicher.** 2005. Continuum description of the cytoskeleton: ring formation in the cell cortex. Phys Rev Lett **95:**258103.

59. **Franz M.R.** Cardiac electrophysiology: from cell to bedside. Zipes D.P., Jalife J., eds. (1995) Philadelphia: WB Saunders. 597–605

60. **Raimond L. Winslow, Anthony L. Kimball, Anthony Varghese, Denis Noble.** 1993. Simulating cardiac sinus and atrial network dynamics on the connection machine. Physica D **64:** 281-298

61. **Kohl, P. and Sachs, F.** (2001). Mechanoelectric feedback in cardiac cells. Philos.Trans. R. Soc. Lond. B Biol. Sci. **359**, 1173-1185.

Vita

Sumeet Kaul was born on April 22nd, 1985 in Chennai, India to Kavitha and Satish Kaul. He has a younger sister, Moneca. In 2002, Sumeet graduated from Sri Chaitanya Junior Colleger in Hyderabad, India. Upon completing his secondary education, he enrolled in the Bachelors of Technology program with concentration in Biomedical Engineering at Jawaharlal Nehru Technological University in Hyderabad, India. In 2006, Sumeet graduated from his Bachelors program. He then decided to continue his education at the University of Tennessee, Knoxville. In the spring of 2007, Sumeet began his graduate studies in biomedical engineering with emphasis in biomechanics, and was supported by a graduate assistantship at the UT RecSports Department. He intends to continue his study and complete his MBA degree at the University of Tennessee's business school.